NASA/TM-20210011810

Micromechanics-Based Modeling of Laminated SiC/SiC Ceramic Matrix Composites

Subodh K. Mital
The University of Toledo, Toledo, Ohio

S.M. Arnold, P.L.N. Murthy, and B.A. Bednarcyk
Glenn Research Center, Cleveland, Ohio

April 2021

NASA STI Program . . . in Profile

Since its founding, NASA has been dedicated to the advancement of aeronautics and space science. The NASA Scientific and Technical Information (STI) Program plays a key part in helping NASA maintain this important role.

The NASA STI Program operates under the auspices of the Agency Chief Information Officer. It collects, organizes, provides for archiving, and disseminates NASA's STI. The NASA STI Program provides access to the NASA Technical Report Server—Registered (NTRS Reg) and NASA Technical Report Server—Public (NTRS) thus providing one of the largest collections of aeronautical and space science STI in the world. Results are published in both non-NASA channels and by NASA in the NASA STI Report Series, which includes the following report types:

- TECHNICAL PUBLICATION. Reports of completed research or a major significant phase of research that present the results of NASA programs and include extensive data or theoretical analysis. Includes compilations of significant scientific and technical data and information deemed to be of continuing reference value. NASA counter-part of peer-reviewed formal professional papers, but has less stringent limitations on manuscript length and extent of graphic presentations.

- TECHNICAL MEMORANDUM. Scientific and technical findings that are preliminary or of specialized interest, e.g., "quick-release" reports, working papers, and bibliographies that contain minimal annotation. Does not contain extensive analysis.

- CONTRACTOR REPORT. Scientific and technical findings by NASA-sponsored contractors and grantees.

- CONFERENCE PUBLICATION. Collected papers from scientific and technical conferences, symposia, seminars, or other meetings sponsored or co-sponsored by NASA.

- SPECIAL PUBLICATION. Scientific, technical, or historical information from NASA programs, projects, and missions, often concerned with subjects having substantial public interest.

- TECHNICAL TRANSLATION. English-language translations of foreign scientific and technical material pertinent to NASA's mission.

For more information about the NASA STI program, see the following:

- Access the NASA STI program home page at http://www.sti.nasa.gov

- E-mail your question to help@sti.nasa.gov

- Fax your question to the NASA STI Information Desk at 757-864-6500

- Telephone the NASA STI Information Desk at 757-864-9658

- Write to:
  NASA STI Program
  Mail Stop 148
  NASA Langley Research Center
  Hampton, VA 23681-2199

NASA/TM-20210011810

Micromechanics-Based Modeling of Laminated SiC/SiC Ceramic Matrix Composites

Subodh K. Mital
The University of Toledo, Toledo, Ohio

S.M. Arnold, P.L.N. Murthy, and B.A. Bednarcyk
Glenn Research Center, Cleveland, Ohio

National Aeronautics and
Space Administration

Glenn Research Center
Cleveland, Ohio 44135

April 2021

This work was sponsored by the
Transformative Aeronautics Concepts Program.

Level of Review: This material has been technically reviewed by technical management.

Available from

NASA STI Program
Mail Stop 148
NASA Langley Research Center
Hampton, VA 23681-2199

National Technical Information Service
5285 Port Royal Road
Springfield, VA 22161
703-605-6000

This report is available in electronic form at http://www.sti.nasa.gov/ and http://ntrs.nasa.gov/

Micromechanics-Based Modeling of Laminated SiC/SiC Ceramic Matrix Composites

Subodh K. Mital
The University of Toledo
Toledo, Ohio 43606

S.M. Arnold, P.L.N. Murthy, and B.A. Bednarcyk
National Aeronautics and Space Administration
Glenn Research Center
Cleveland, Ohio 44135

Abstract

The behavior and response of ceramic matrix composites (CMCs), in particular silicon carbide fiber reinforced silicon carbide matrix (SiC/SiC), is affected by many factors such as variation of fiber volume fraction, residual stresses resulting from processing of the composites at high temperature, random microstructures, and the presence of matrix flaws (e.g., voids, pores, cracks, etc.) as well as general material nonlinearity and heterogeneity that occurs randomly in a composite. Residual stresses arising from the phase change of constituents are evaluated in this paper and it is shown that they do influence composite strength and need to be properly accounted for. Additionally, the microstructures (location of fiber centers, coating thickness, etc.) of advanced CMCs are usually disordered (or random) and fiber diameter and strength typically have a distribution. They rarely resemble the ordered fiber packing (square, rectangular, or hexagonal) that is generally assumed in micromechanics-based models with periodic boundary conditions for computational expediency. These issues raise the question of how should one model such systems effectively? Can an ordered hexagonal packed repeating unit cell (RUC) accurately represent the random microstructure behavior? How many fibers need to be included to enable accurate representation? Clearly, the number of fibers within an RUC must be limited to insure a balance between accuracy and efficiency. NASA's in-house micromechanics-based code MAC/GMC provides a framework to analyze such RUCs for the overall composite behavior and the FEAMAC computer code provides linkage of MAC/GMC to the commercial FEA code, ABAQUS. The appropriate level of discretization of the RUC as well as the analysis method employed, i.e., Generalized Method of Cells (GMC) or High Fidelity Generalized Method of Cells (HFGMC), is investigated in this paper in the context of a unidirectional as well as a cross-ply laminated CMC. Results including effective composite properties, proportional limit stress (an important design parameter) and fatigue are shown utilizing both GMC as well as HFGMC. Finally, a few multiscale analyses are performed on smooth bar test coupons as well as test coupons with features such as open-hole and double notches using FEAMAC. Best practices and guidance are provided to take these phenomena into account and keep a proper balance between fidelity (accuracy) and efficiency. Following these guidelines can account for important physics of the problem and provide significant advantages when performing large multiscale composite structural analyses.

Introduction

Advanced ceramic matrix composites (CMCs) are being aggressively pursued as potential candidates for many aerospace applications as they offer a unique combination of high temperature strength, creep resistance, low density, high thermal conductivity and low thermal expansion. Residual stresses can occur in CMCs due to the difference in coefficient of thermal expansion (CTE) of various constituents, ply layers and/or constituent phase changes within the composite. Since both fiber and matrix are silicon carbide based, the CTE mismatch is usually minimal. In melt-infiltrated (MI) SiC/SiC composites, the preform is infiltrated with molten silicon to create a dense composite. The silicon reacts with carbon in the preform to create a reaction-formed silicon carbide (SiC) matrix. However, there is always some excess silicon in the matrix referred to as free silicon. This free silicon goes through a phase change during the processing of the composite and results in residual stresses in the as-fabricated composite. The resulting residual stress influences both the composite proportional limit stress (PLS) as well as the ultimate tensile strength (UTS). PLS, also referred to as the matrix-cracking stress is a very important design parameter, since matrix cracks provide a path for the atmosphere to degrade the fiber matrix interface and fiber strength. It is believed that PLS will be the upper limit of the allowable CMC stress for long life applications (Ref. 1).

Low fiber volume fraction composite systems like CMCs inherently have more microstructure variations (location of fiber centers – disordered/random packing, coating thickness, etc.) than higher volume fraction polymer matrix composite (PMC) systems. In addition, there is manufacturing variability along the fiber length, such as variable fiber diameter and variable thickness of fiber coatings, thus raising the question of how should one model such systems effectively; i.e., keeping a proper balance between accuracy and efficiency when performing multiscale composite analyses. Clearly, from a computational point of view, it is preferable to keep the number of fibers in a repeating unit cell (RUC) to a minimum. NASA's in-house micromechanics-based code MAC/GMC (Ref. 2) provides a framework to analyze such RUCs for the overall composite behavior. This framework embodies two basic micromechanics models, 1) Generalized Method of Cells (GMC) and 2) High Fidelity Generalized Method of Cells (HFGMC), which provide semi closed-form constitutive equations for composite effective properties, composite response, as well as local (microscale) stress and strain fields in the constituents of the composite. With the increased emphasis on reducing the cost and time to market of new materials, Integrated Computational Materials Engineering (ICME) has become a fast-growing discipline within materials science and engineering. ICME is an integrated approach to the design of products and the materials which comprise them by linking material models at multiple time and length scales; such that manufacturing processes, which produce internal material structures that in turn influence material properties and allowables, can be tailored (engineered) to specific industrial applications. Experimental micrographs of composite microstructures have shown that actual microstructures rarely resemble ordered arrangements and show at least some degree of spatial randomness, although this randomness diminishes as fiber volume fraction increases since fiber movement is more constrained (see Figure 1). However, due to the diminishing effect of microscale randomness at higher length scales, microstructural variability is often ignored and micromechanics-based models assuming periodic boundary conditions, with an ordered array of fibers (either square or hexagonally packed fibers), are typically utilized.

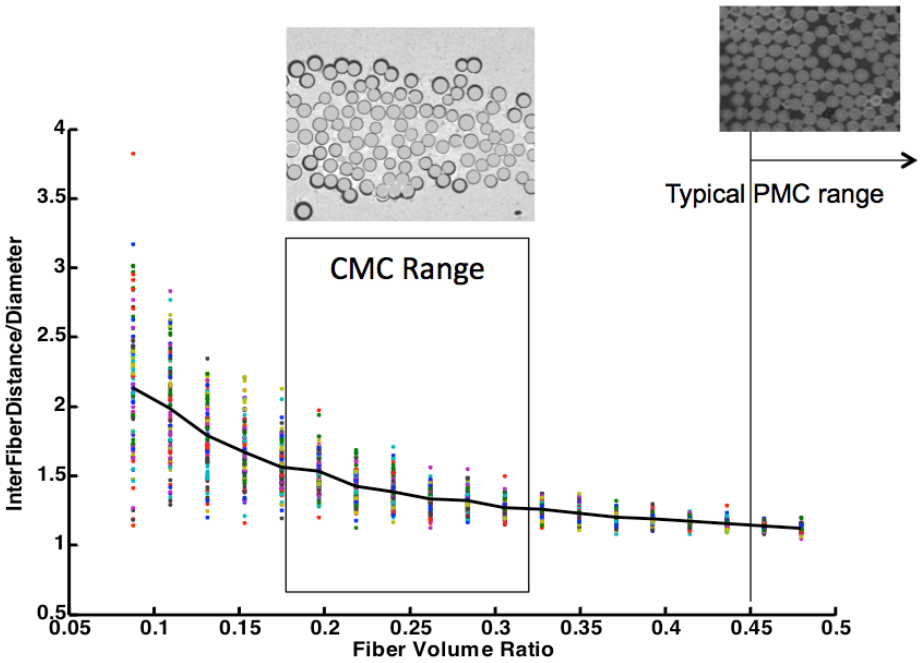

Figure 1.—Measure of fiber movement versus fiber volume fraction. Micrograph for a typical ceramic matrix composite.

Researchers have investigated the effect of random or disordered microstructures on various composite response behaviors, assuming elastic and damage behavior (Refs. 3 to 8). In our previous work (Ref. 9) the influence of ordered and disordered microstructures on the effective properties and fatigue life of graphite/epoxy polymer matrix composite (PMC) at low volume fractions was studied in the context of assessing the advantages/limitations of the micromechanics idealizations (GMC - generalized method of cells or HFGMC – high fidelity generalized method of cells) available within the general, synergistic, multiscale-modeling framework for composites (developed by the NASA Glenn Research Center (GRC)) and known as MAC/GMC and FEAMAC (Ref. 10) when considering microstructural arrangement. This framework can be effectively utilized to link the material microstructure (e.g., constituent phase properties, volume fraction, fiber packing) to ply/laminate properties (mesoscale) and finally to performance (at the macroscale), see Figure 2, in an efficient and accurate manner to enable 'fit-for-purpose' tailoring of the composite material. Finally, a few micromechanics-based multiscale analyses are performed on smooth bar test coupons as well as open-hole and double-notched unidirectional and cross-ply test coupons. Since, these analyses are usually quite resource intense, recommendations are made for selection of a proper RUC with regards to size and details included, as well as the analysis method used. The desire again is to maintain a proper balance between accuracy (fidelity of the model) and efficiency for achieving practical engineering results in a reasonable amount of time to make the tool practical.

The objective of this paper is to summarize our current understanding of: the effect of residual stresses on the composite response, the statistical influence of microstructure (both ordered and disordered) on the overall accuracy of predicted unidirectional and laminated CMCs response for both static and cyclic loading, the advantages/limitations of the micromechanics idealization (GMC or HFGMC), and the influence of lower length scale idealizations on higher scale response in multiscale analyses. A brief background of the generalized method of cells along with details of the continuum damage fatigue model employed are presented in the following sections. Residual stresses that arise due

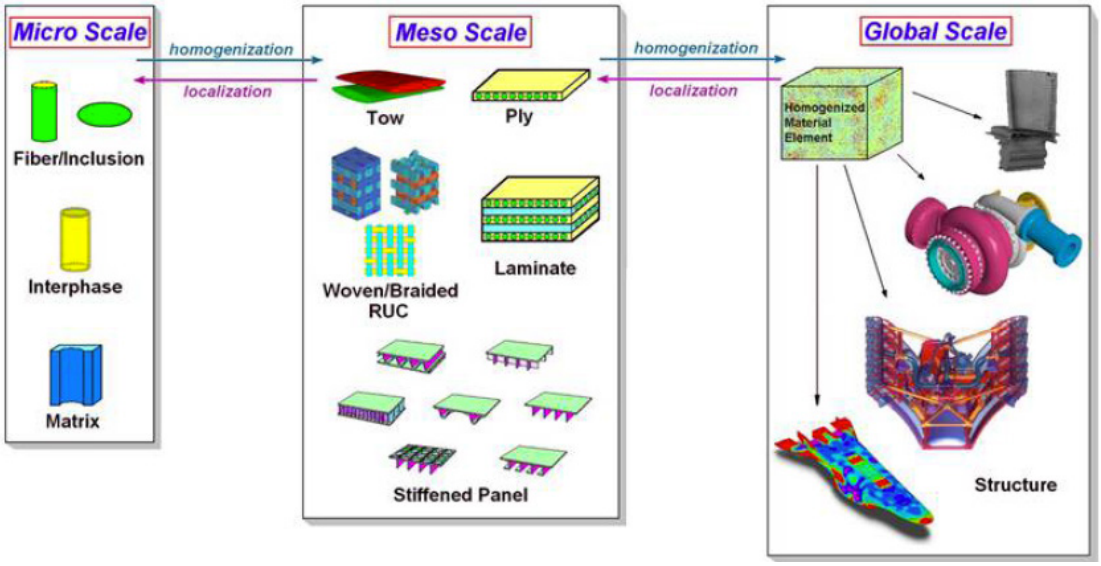

Figure 2.—Illustration of relevant levels of scales for multiscale composite analysis.

to processing are discussed and a general discussion of the RUC based modeling of the ordered and disordered microstructure is presented next. Results for elastic properties, strength and fatigue lives using two micromechanics theories available in MAC/GMC computer code as well as effects of manufacturing variability arising due to the variation in fiber diameter and interface coating thickness are presented next. The paper concludes with some multiscale problems that demonstrate the capability of the MAC/GMC and FEAMAC computer code along with some general concluding remarks.

Generalized Method of Cells

GMC, first developed by Paley and Aboudi (Ref. 11) and HFGMC, first developed by Aboudi et al. (Ref. 12), are semi-analytical in nature, and their formulation involves application of several governing conditions in an average sense. They provide the local fields in composite materials, allowing incorporation of arbitrary inelastic constitutive models with various deformation and damage constitutive laws (Ref. 10). The microstructure of a periodic multiphase material, within the context of GMC and HFGMC, is represented by a doubly-periodic (continuously reinforced) or triply-periodic (discontinuously reinforced) RUC consisting of an arbitrary number of subcells, each of which may be a distinct material (Figure 3). In the case of GMC the displacement field is assumed linear, whereas in the case of HFGMC the displacement approximations are assumed quadratic, thus leading to a constant and linear subcell strain field, respectively. In fact, it is precisely this higher order assumption in the displacement field that enables HFGMC to retain its ability to compute nonzero transverse shear stress distributions within the composite (i.e., normal and shear coupling), which is so important when dealing with disordered microstructures (Refs. 10, 12, and 13). However, it is also this high-order field assumption which makes HFGMC more computationally expensive (Refs. 10 and 14) and subject to subcell discretization dependence as compared to GMC.

Displacement and traction continuity are enforced in an average, or integral sense at each of the subcell interfaces and the periodic boundaries of the RUC. These continuity conditions are used to formulate a strain concentration matrix $\mathbf{A}$, which gives all the local subcell strains (ϵ_S) in terms of the global, average, applied strains $\epsilon_{applied}$ (i.e., $\epsilon_S = \mathbf{A}\,\epsilon_{applied}$). The local subcell stresses (σ) can then be calculated using the local constitutive law and the local subcell strains. Finally, the overall RUC stiffness

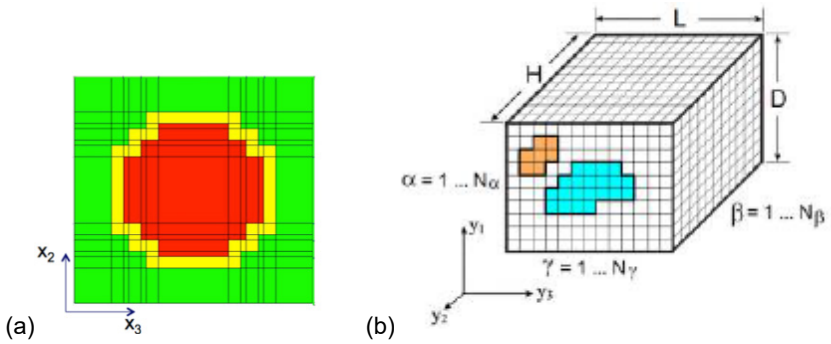

Figure 3.—Composite with repeating microstructure and arbitrary constituents. (a) Doubly periodic, and (b) Triply periodic.

is obtained utilizing the local constitutive law and the strain concentration matrix averaged over the RUC dimensions. The detailed methodology of GMC and HFGMC and the formulation to be embedded within classical laminate theory is described thoroughly in Aboudi et al. (Refs. 10 and 14). Also, in these references the superior accuracy of HFGMC over that of GMC is demonstrated, consequently in this study HFGMC will be assumed to provide the most accurate predictions.

Constitutive Models

The most well-known and widely used constitutive model is Hooke's law is written as

$$\sigma_{ij} = C_{ijkl}\,\varepsilon_{kl} \tag{1}$$

which describes time-independent, linear (proportional) reversible material behavior, where C_{ijkl} is the classic stiffness tensor and ε_{kl} is the elastic component of the strain tensor. Extension into the irreversible regime has been accomplished by assuming an additive decomposition of the total strain tensor into three components, that is a reversible mechanical strain (i.e., elastic/viscoelastic) ε_{ij}; an irreversible (i.e., inelastic or viscoplastic) strain ε_{ij}^{I}; and a reversible thermal strain, ε_{ij}^{th} component.

$$\varepsilon_{ij}^{total} = \varepsilon_{ij} + \varepsilon_{ij}^{I} + \varepsilon_{ij}^{th} \tag{2}$$

or

$$\varepsilon_{ij} = \varepsilon_{ij}^{total} - \varepsilon_{ij}^{I} - \varepsilon_{ij}^{th} \tag{3}$$

After substituting expression (3) into Equation (1) we arrive at a stress strain relation (generalized Hooke's law) that incorporates irreversible strains as well as reversible ones, that is:

$$\sigma_{ij} = C_{ijkl}(\varepsilon_{kl} - \varepsilon_{kl}^{I} - \varepsilon_{kl}^{th}) \tag{4}$$

where numerous models describing the evolution of the inelastic strain have been proposed in the literature (Refs. 15 to 17).

Deformation Model

Constituent deformation behavior is assumed to follow Hooke's Law up to failure. The elastic properties of all three constituent materials (Hi-Nicalon Type-S fiber, BN coating and SiC matrix) are given in Table I. These properties have been assumed based on internal discussions with the ceramic materials researchers. The matrix (represented by green subcells), the fiber (represented by red subcells) and the explicit interface coating (represented by yellow subcells) in Figure 3(a) are all assumed isotropic; with Young's modulus (E_m, E_f, E_c) and Poisson's ratio (ν_m, ν_f, ν_c) along with the associated shear modulus (G_m, G_f, G_c) all given in Table I. Note the ratio of constituent properties are $E_f/E_m = 1.18$; $E_c/E_m = 0.03$; $G_f/G_m = 1.23$; $G_c/G_m = 0.03$. All constituents are assumed to be brittle and the static failure of each constituent is assumed to be governed by the maximum stress criterion (both normal (σ_u) and shear (τ)) with the strengths given in Table I. The proportional limit stress (PLS) is determined from the global stress-strain curve by assuming the CMC community accepted 0.005 percent total strain off-set from the origin. Temperature dependent constituent elastic and creep properties are given in Table II wherein creep (ε_{ij}^I) is idealized using an isotropic Norton-Bailey power law creep model (Ref. 17). Norton-Bailey power law for uniaxial creep can be written as:

$$\frac{d\varepsilon^I}{dt} = A\sigma^n \tag{5}$$

where A and n are required isotropic parameters of this model and σ is the stress and t is time. A multiaxial form of this law, known as Odquist model can be written as:

$$\frac{d\varepsilon_{ij}^I}{dt} = BJ_2^m S_{ij} \tag{6}$$

where $m = \frac{1}{2}(n-1)$ and $B = \frac{1}{2}\left(3^{\frac{n+1}{2}}\right)A$ and $J_2 = \frac{1}{2}S_{ij}S_{ij}$ with $S_{ij} = \sigma_{ij} - \frac{1}{3}\sigma_{kk}\delta_{ij}$.

As shown, the parameters of the multiaxial creep law can be computed from the parameters of the uniaxial creep model A and n. It should also be noted that monotonic failure is accounted for with the failure stress shown in Table I.

TABLE I.—CONSTITUENT (FIBER/MATRIX/COATING) ELASTIC PROPERTIES

Hi-Nicalon Type S Fiber	BN - Coating	SiC matrix
E_f=385.0 GPa	E_c =10.0 GPa	E_m =327.0 GPa
ν_f =0.17	ν_c =0.23	ν_m =0.22
G_{f23} = 164.53 GPa	G_{c23} =4.07 GPa	G_{m23} = 134.0 GPa
σ_{uf} = 1800 MPa	σ_{uc} = 70 MPa	σ_{um} = 600 MPa
τ_f = 700 MPa	τ_c = 45 MPa	τ_m = 350 MPa

TABLE II.—TEMPERATURE DEPENDENT CONSTITUENT MATERIAL PROPERTIES

Model parameter	RT	1,100 °C	1,200 °C	1,300 °C	1,400 °C
Hi–Nic Type S Fiber					
Young's modulus, E, GPa	385.0	375.0	370.0	365.0	365.0
Poisson's ratio, ν_{12}	0.17	0.17	0.17	0.17	0.17
Coefficient of thermal expansion, α, 10^{-6}/°C	3.2	5.5	5.5	5.5	5.5
A, MPa^{-3} hr	0	3.32×10^{-17}	1.68×10^{-13}	2.76×10^{-13}	5.17×10^{-13}
n	3	3	3	3	3
BN – Coating					
Young's modulus, E, GPa	10	9	9	9	9
Poisson's ratio, ν_{12}	0.22	0.22	0.22	0.22	0.22
Coefficient of thermal expansion, α, 10^{-6}/°C	4.0	5.5	5.5	5.5	5.5
SiC matrix					
Young's modulus, E, GPa	410.0	400.0	390.0	385.0	380.0
Poisson's ratio, ν_{12}	0.17	0.17	0.17	0.17	0.17
Coefficient of thermal expansion, α, 10^{-6}/°C	3.1	5.5	5.5	5.5	5.5
A, MPa^{-3} hr	0	2.55×10^{-11}	2.04×10^{-9}	1.02×10^{-8}	4.31×10^{-8}
n	1.5	1.5	1.5	1.5	1.5
Free silicon					
Young's modulus, E, GPa	160.0	155.0	153.0	150.0	150.0
Poisson's ratio, ν_{12}	0.24	0.24	0.24	0.24	0.24
Coefficient of thermal expansion, α, 10^{-6}/°C	3.0	6.0	6.0	6.0	6.0
A, MPa^{-3} hr	0	5.08×10^{-10}	4.06×10^{-8}	2.03×10^{-7}	8.6×10^{-7}
n	1.3	1.3	1.3	1.3	1.3

$A(T)$ and n are creep parameters

Continuum Fatigue Damage Model

The fatigue life of the composite will be predicted utilizing micromechanics and the isotropic form of the multiaxial, isothermal, continuum damage mechanics model of Arnold and Kruch (Ref. 18) for the matrix constituent. When reduced to its isotropic form (parameters ω_u, ω_{fl}, ω_m, η_u, η_{fl}, and η_m set equal to one) this model reduces to the Non-Linear Cumulative Damage Rule (NLCDR) developed at ONERA (Ref. 19). This model assumes a single scalar internal damage variable, D, that has a value of zero for undamaged material and one for a completely damaged (failed) material. The implementation of the damage model within GMC and HFGMC has been performed on the local scale, thus damage evolves in each subcell based on the local stress state and number of cycles. For a given damage level, the stiffness of the subcell is degraded by $(1 - D)$. Further, the implementation allows the application of a local damage increment ΔD, and then calculates the number of cycles, N, required to achieve this local increment of damage. This approach allows the model to determine the stress state in the composite, identify the controlling subcell that will reach the desired damage level in the fewest cycles, apply that number of cycles to all subcells, and calculate the damage that arises throughout the remainder of the composite. Then the composite can be reanalyzed, and a new stress state determined based on the new, spatially varying, damage level throughout the composite RUC. In this way, the local and global stress

and damage analyses are coupled. As the damage in the composite evolves, the stress field in the composite is redistributed, which then affects the evolution of damage. It should be noted that the monotonic failure is accounted for by specifying the maximum allowable stresses shown in Table I.

For an isotropic material, the damage parameters that must be selected reduce to M, β, and a, while the pertinent equation relating the fatigue life of the isotropic material to the cyclic stress state is,

$$N_F = \frac{\left(\sigma_u - \sigma_{\max}\right)\left(\dfrac{M}{\sigma_{\max} - \bar{\sigma}}\right)^{\beta}}{\hat{a}\left(1+\beta\right)\left(\sigma_{\max} - \bar{\sigma} - \sigma_{fl}\right)} \qquad \text{for} \qquad N_F > 0 \tag{7}$$

where σ_u is the material ultimate strength, σ_{fl} is the material fatigue limit (stress below which damage does not occur), $\sigma_{\max}$ is the maximum stress during a loading cycle, $\bar{\sigma}$ is the mean stress during a loading cycle, and N_F is the number of cycles to failure. Note that, in the terminology of Arnold and Kruch (Ref. 18), $\hat{a} = a\frac{\sigma_{fl}}{\sigma_u}$. Utilizing Equation (5), the damage model parameters M, β and a can be selected for an isotropic material based on the material's S-N curve (stress level vs. cycles to failure). Both the fatigue limit and the scaling parameter M are general enough to account for the effect of mean stress. However, in this study this additional effect is ignored since only one R ratio (R = –1, fully reversed) is examined. A representative S-N curve for a SiC matrix was obtained, and the corresponding fatigue damage model parameters were found to be M = 550 MPa, β = 8, and a = 0.4, with σ_u = 600 MPa, and σ_{fl} = 65.0 MPa. A plot showing the resulting matrix S-N curve is given in Figure 4. Note the dotted line illustrates how the above function behaves below a single cycle yet static fracture would occur at 600 MPa (as indicated by the x in Figure 4).

A second damage model within GMC and HFGMC is much simpler and involves degradation of a material's strength due to cyclic loading. As shown by Wilt et al. (Ref. 20), this type of damage model can be used to simulate the fatigue behavior of fibers that occurs in-situ during fatigue of a composite. The model assumes a logarithmic relation between the material's strength and the number of cycles within a certain range such that:

$$\begin{aligned} \sigma_u &= \sigma_{u1} && 0 \le N \le N_1 \\ \sigma_u &= \sigma_{u1} - \frac{\left(\sigma_{u1} - \sigma_{u2}\right)\log\left(N/N_1\right)}{\log\left(N_2/N_1\right)} && N_1 \le N \le N_2 \\ \sigma_u &= \sigma_{u2} && N_2 \le N \end{aligned} \tag{8}$$

This strength degradation model (Eq. (6)) was employed in the present example to model the longitudinal fatigue behavior of the graphite fiber. The necessary parameters for the model are σ_{u1}, σ_{u2}, N_1, and N_2. The values of these parameters chosen for the Hi-NiC Type-S fiber are shown in Figure 5. Note that these data were not correlated with experiment, but rather chosen based on the expected trend. Given these required parameters for the fatigue damage models for each phase in the SiC/SiC composite, macroscopic or composite fatigue life of both unidirectional and [0/90] cross-ply composite laminates can be simulated. Note although creep-fatigue interaction can be incorporated in the above theory, see (Ref. 21), it is not included in the present calculations.

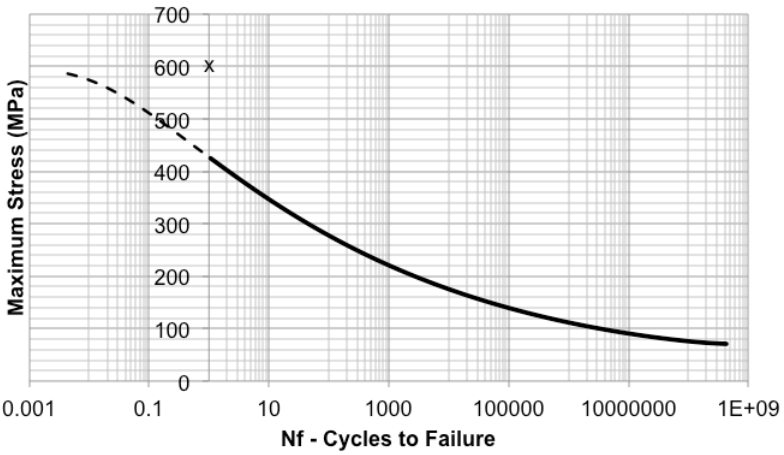

Figure 4.—Stiffness reduction fatigue damage model representation for in-situ SiC matrix.

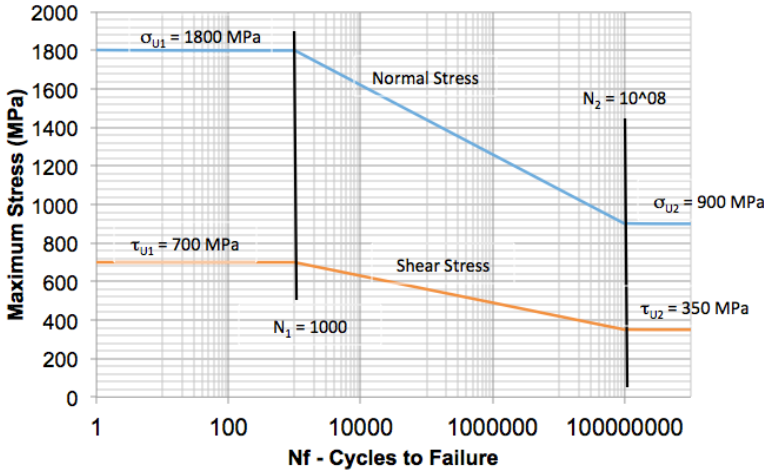

Figure 5.—Strength reduction fatigue model parameters assumed for the Hi-NiC Type-S fiber.

Results/Discussion

Residual Stresses

Composite materials usually develop residual stresses as a result of processing. Advanced CMCs are processed at a high temperature and the composite is cooled down following some time-temperature profile. Since composite constituents can have different coefficients of thermal expansions as well as different creep/relaxation rates, there is a constant stress redistribution (load shedding) from one constituent to another that results in residual stresses developing within the composite in the as-fabricated condition. Residual stresses are important and need to be accounted for as they affect the PLS and UTS of the composite material. In the case of SiC/SiC CMCs, residual stresses arising from the mismatch between the constituents' thermal expansion coefficients are minimal, as both the fiber and matrix are silicon carbide-based constituents. However, there is usually enough free silicon (Si) within the matrix (which goes through a phase change) that gives rise to residual stresses in the fiber and matrix due to processing. This is particularly true in the MI SiC/SiC composites being analyzed herein. A previous

method employed to include such residual stresses in the CMC predictions involved performing separate uncoupled homogenization between free silicon and SiC matrix to get an effective recrystallization strain. An equivalent recrystallization coefficient (CXE) for the homogenized matrix was computed and artificially adjusted to match the composite stress-strain curves and to account for any relaxation that takes place during the processing of the composite. However, the value chosen of the CXE is arbitrary (Ref. 22). This approach is fine for a purely elastic analyses as it merely requires knocking down (adjusting) the recrystallization strain to get more realistic residual stresses. However, time-dependent effects or interactions between the free silicon and SiC are missing. Thus, any time-dependent effect, such as temperature rate changes or any post-processing heat treatment preformed on the composite, that will change the residual stresses cannot really be accounted for. Consequently, an alternate approach used herein is to assume a process history, account for the stresses resulting from the phase change, and account for the creep/relaxation of the constituents with time, temperature and stress. This process explicitly computes the residual stresses resulting from applying this process history while considering the creep/relaxation in various constituents. This approach can also account for any heat treatment that may be performed as a post-processing step.

To demonstrate this approach using NASA's MAC/GMC computer code, a sample processing history along with a heat treatment performed after the processing but prior to any application of mechanical load is shown schematically in Figure 6. A simple power law for the creep/relaxation of the form $\varepsilon' = A\,\sigma^n$ available in MAC/GMC is used. Constituent properties as a function of temperature as well as parameters for power-law creep are shown in Table II. Figure 7 shows the qualitative effect on the [0/90] laminate baseline case room-temperature tensile response. The inclusion of residual stresses or any subsequent heat treatment does not change the initial elastic modulus but does influence predicted the PLS as well as the UTS (ultimate tensile strength). When the residual stresses are included, the PLS increases and the UTS is reduced (due to pre-straining of the fiber). As mentioned before, since PLS is the upper limit of allowable CMC stress, increasing the PLS of the composite has a beneficial effect in that the allowable stresses on the composite increase. When a heat treatment is performed after the processing but prior to any application of mechanical loads, the PLS decreases and the UTS increases as shown in Figure 7. The exact magnitude of change is dependent upon dwell time at temperature, e.g., dwell of 10,000 hr at 1,100 °C shows greater decrease (see purple line, Figure 7) in PLS than does 100 hr (green line). Consequently, the micromechanics analyses performed using MAC/GMC can account for any time related effects on the composite response.

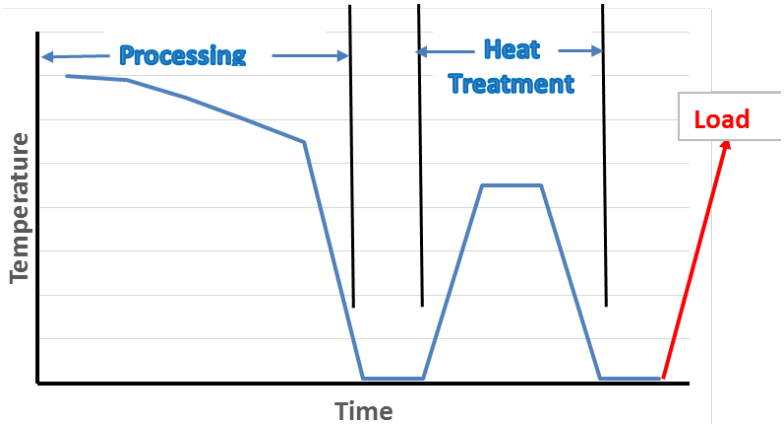

Figure 6.—A schematic of a processing history and a subsequent heat treatment applied prior to an application of a mechanical load

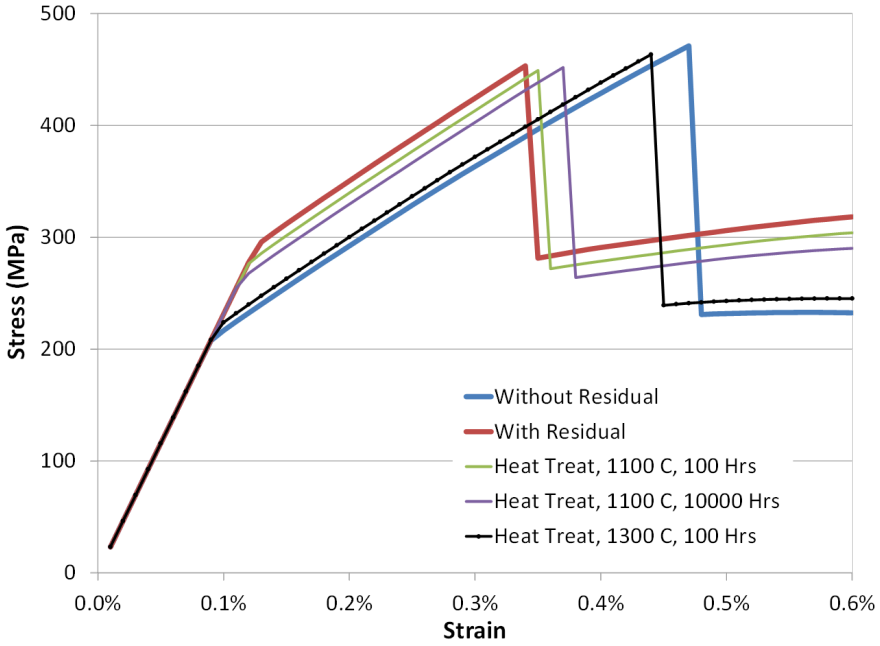

Figure 7.—Qualitative effects of heat treatment on [0/90] laminate room-temperature tensile response.

RUC-Based Modeling in the Presence of Random Microstructures

In a previous paper (Ref. 9), the statistical influence of microstructure (both ordered and disordered) on the unidirectional and laminated composite effective properties and fatigue life for a graphite/epoxy polymer matrix composite with strong interface was investigated. It was determined that accounting for spatial variations in composite microstructure enables one to simulate observed statistical variations in both effective properties and fatigue life. However, the more computationally efficient GMC is significantly less sensitive to microstructure variations than is HFGMC. GMC typically predicted lower effective properties and higher fatigue lives than did HFGMC for ordered microstructures. Fatigue lives for RUCs representing ordered microstructures with GMC were also higher and significantly outside the range of those lives computed for RUCs with disordered microstructures; whereas fatigue lives predicted with ordered RUCs using HFGMC were within the range of those lives determined using disordered microstructures. Further, although fatigue lives predicted by HFGMC vary significantly based on individual microstructures (whereas GMC is relatively insensitive), the mean life value (i.e., averaged over multiple microstructure realizations) for a given RUC discretization between HFGMC and GMC was shown to be relatively small (< 30 percent) compared to lives produced using an ordered (single fiber with periodic boundary conditions) microstructure. Note that the actual percentage discrepancy, in the case of disordered microstructures, is highly dependent upon volume fraction and property mismatch between constituents.

In this paper, we again examine the influence of micromechanics idealization (GMC and HFGMC), for both ordered and disordered microstructures, on the unidirectional and laminated composite effective properties, PLS and fatigue life, but this time for a ceramic matrix composite (CMC) with an explicit weak interface. The fiber and interface volume fractions being held fixed at 28 and 13 percent, respectively, and the constituent properties are assumed to be deterministic throughout this study. In order to evaluate the influence of microstructural variation only, residual stresses are not included in this part of the work.

GMC and HFGMC RUC and Subcell Refinement: Ordered Microstructures

The various ordered RUCs considered are shown in Figure 8. Figure 9 illustrates the influence of subcell and RUC refinement on the effective tensile and shear moduli, PLS, and fatigue life for four different circular fiber RUCs; RUC-D, -E, -F and -Base shown in Figure 8. Clearly, no subcell discretization dependence is observed for GMC, provided the RUC remains fixed (see RUC-D, -E, -F in Figure 8), irrespective of response parameter examined. It should be mentioned that finite element analyses show mesh dependency. GMC has no mesh dependency because of the assumptions used in the theory i.e. decoupling of normal and shear stresses. However, if the circular fiber representation changes (e.g., RUC-D versus RUC-Base) then both deformation and life (to a greater extent) response are affected. HFGMC does exhibit subcell discretization and aspect ratio dependence (due to coupling of normal and shear stresses) wherein one sees that the transverse normal and transverse shear modulus and PLS are slightly impacted; while the transverse fatigue life (Figure 9(d)), is significantly affected as it depends more heavily on the accuracy of the local fields. This is expected since GMC is a first order theory (so that fiber volume fraction of a given constituent per row or column in an RUC matters (Ref. 13)), whereas HFGMC is a second order theory that enables normal shear coupling, see (Ref. 10 and 14).

Comparing the difference between effective composite properties predicted by HFGMC and GMC (typically under predicting), one sees approximately a 13 percent difference in transverse normal stiffness, 20 percent in longitudinal shear and 40 percent difference in transverse shear modulus. GMC typically predicted longer lives than did HFGMC for a corresponding RUC idealization; the difference being almost a factor of 2 for the RUC-Base. Similarly, we see that the fatigue life computed by HFGMC for RUC-Base is approximately half that of RUC-E. Note, although HFGMC is considered more accurate then GMC, on average it is orders of magnitudes slower than GMC. Therefore, in large structural problems it is important to balance computational efficiency with fidelity (accuracy), particularly in the case of fatigue life calculations.

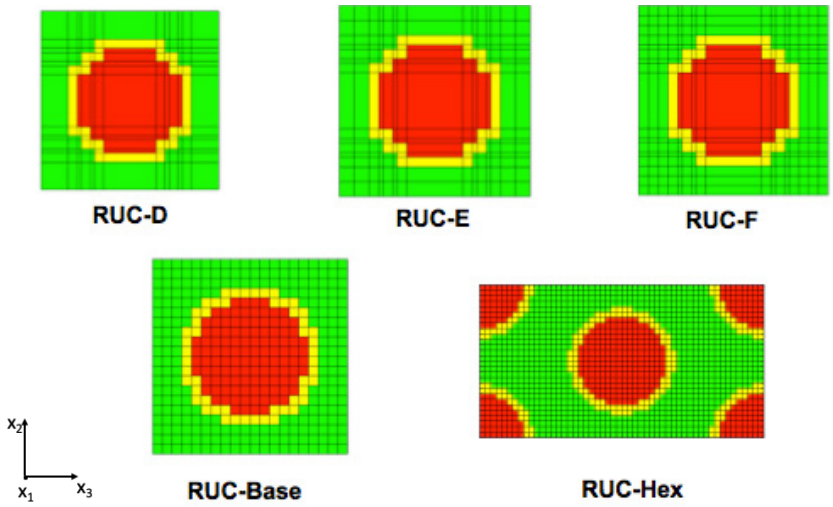

Figure 8.—Ordered Repeating Unit Cells where for the square packed architectures matrix discretization is the difference between RUC-D, -E, and –F , i.e., 2, 4 and 6 subcells between fibers, respectively, while RUC-Base has a uniform subcell discretization (i.e., subcell aspect ratio of one).

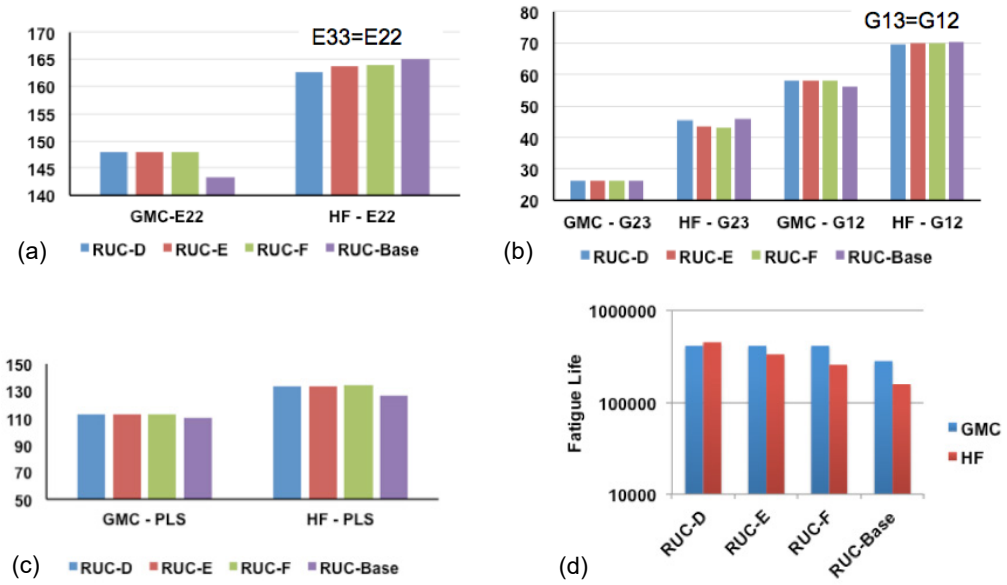

Figure 9.—Influence of Subcell Refinement, given circular fiber RUC, on the effective property, PLS and fatigue life (σ_{max} = 52 MPa, R = -1) predicted by GMC and HFGMC. (a) Tensile modulus, (b) shear moduli, (c) proportional limit stress, and (d) fatigue life: fully reversed 52 MPa.

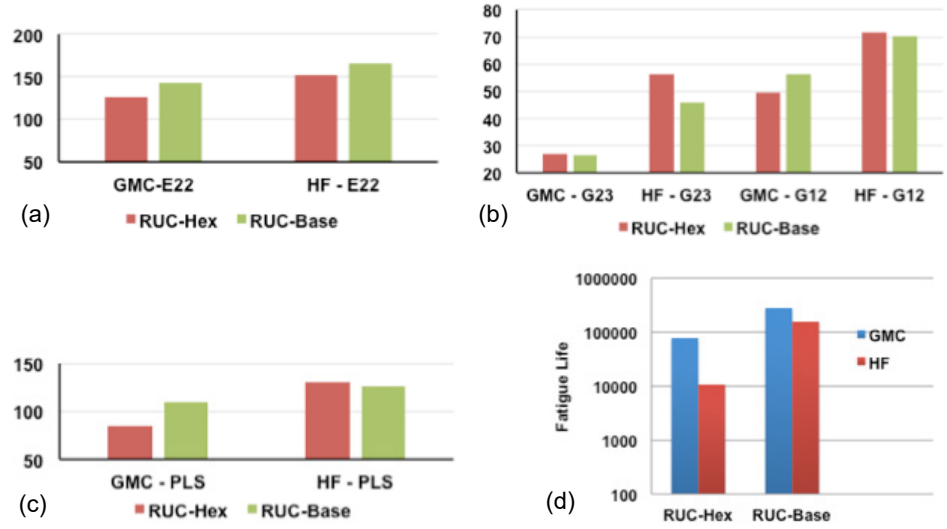

Figure 10.—Influence of ordered fiber packing arrangements; hexagonal versus square (see Figure 7). (a) Tensile modulus, (b) shear moduli, (c) proportional limit stress, and (d) fatigue life: fully reversed 52 MPa.

Figure 10 illustrates the difference in effective tensile and shear moduli, PLS, and fatigue life between two ordered microstructures; a square packed (RUC-Base) and hexagonal packed (RUC-Hex, see Figure 8) fiber architecture. Comparing the difference between hexagonal packed effective composite properties predicted by HFGMC and GMC (typically under predicting), one sees approximately a 17 percent difference in transverse normal stiffness (note for GMC $E_{33} \neq E_{22}$ for RUC-Hex), 30 percent in longitudinal shear (note for GMC $G_{13} \neq G_{12}$ for RUC-Hex), and 50 percent difference in transverse shear modulus, see (Ref. 14) for more details. In case of failure the difference in hexagonal packing between

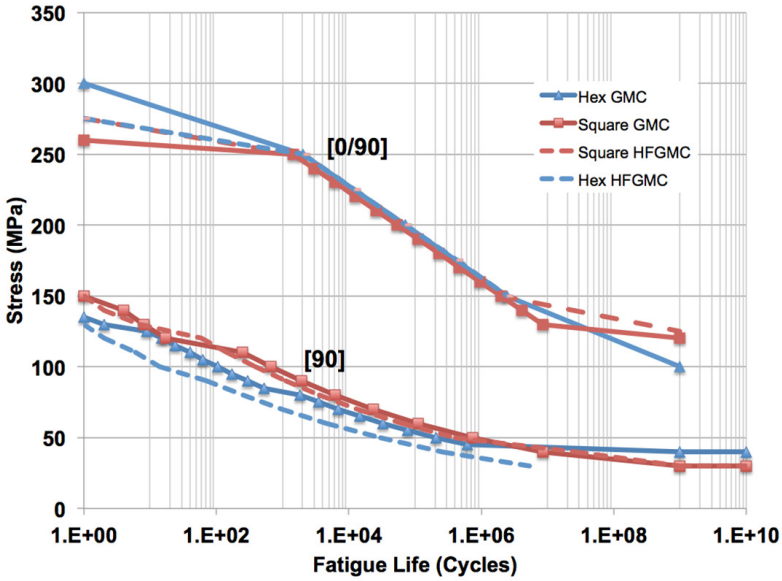

Figure 11.—S-N curves for two ordered microstructures containing: square and hexagonal fiber packing architecture.

methods is significantly greater than for square, with the PLS being approximately 30 percent and fatigue life 600 percent. It is interesting to note that the difference between packing arrangements for GMC is significantly more than it is for HFGMC due to the presence of the weak interface and lack of normal-shear coupling that is inherent to GMC micromechanics. Finally in Figure 11 stress level versus fatigue life cycles (S-N curves) for a unidirectional laminate loaded transverse to fibers, i.e., [90] and a symmetric cross-ply laminate, $[0/90]_s$, are shown, given these two different packing arrangements. Most notable is the significant variation in both packing and method for the [90] laminate as compared to the $[0/90]_s$. This clearly illustrates that microstructure variation is significantly reduced by the presence of [0] plies within the laminate since longitudinal (fiber direction) response is predominately influenced by the fiber behavior. Furthermore, differences between micromechanics methods are also minimized when predicting laminates containing zero plies, see (Ref. 14) for a detailed discussion of progressive damage under static loading.

Ordered Versus Disordered Microstructure

Realistic composite microstructures typically are not well ordered, particularly in the case of CMCs, which have lower fiber volume fractions of less than 35 percent and thus more opportunity for fiber movement. Consequently, it is important to understand the influence of random fiber placement (disordered microstructure) on the deformation (effective properties, PLS) and failure (e.g., fatigue life) behavior of the composite. Given the above results, the 20x20 RUC-Base (see Figure 8) was selected as our fundamental building block for generating an RUC containing more than a single fiber. Multiple fiber RUC studies containing 4, 25 and 100 fibers in an RUC were conducted to evaluate the effects of random fiber distributions as well as to decide how many fibers one should use in an RUC with random microstructure and yet maintain a proper balance between efficiency (CPU time) and accuracy (some measure of error). Figure 12 shows average values of in-plane transverse modulus, E_{22} and in-plane shear modulus, G_{12} for a [90] laminate as a function of number of fibers in the RUC using HFGMC micromechanics analyses using random fiber placement. Results are based on 100 simulations for each case. Properties are normalized by the average values of HFGMC analyses with an RUC containing 100 fibers. It also shows normalized computational time normalized by the CPU time required for a HFGMC

analysis for a square pack RUC (0.127 sec). For comparison, CPU time taken for a regular Hex pack HFGMC analysis is 0.51 sec on a standard stand-alone PC. Results show that when you change the random RUC from 4 to 9 fibers, the computational cost increases by approximately three times while the improvement in accuracy is less than 2 percent. For RUCs containing 16, or more fibers, the computational costs increase exponentially. Based on these observations, it was decided to utilize a 40x40 four fiber RUC consisting of a total number of 1600 subcells as our baseline multi-fiber RUC to study the effects of random fiber distribution. Ten samples of four-fiber RUCs out of the 100 randomly generated and analyzed instances are shown in Figure 13. The nominal fiber and BN coating volume fractions are 28 and 13 percent, respectively. Constituent material properties remain the same as given in Table I.

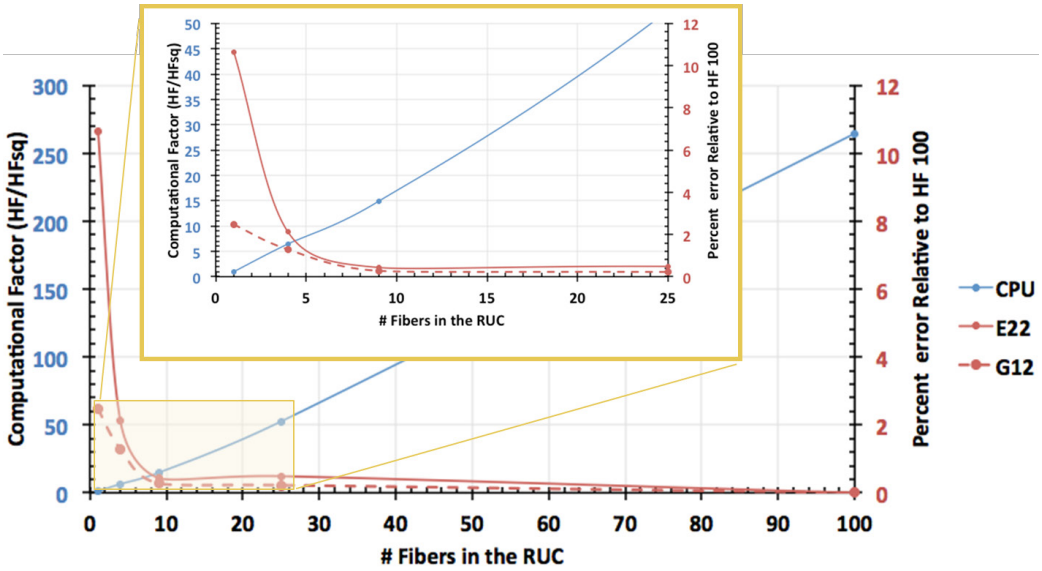

Figure 12.—HFGMC results for a [90] laminate for average values of transverse modulus and in-plane shear modulus as well as the normalized computational cost. Results are based on 100 simulations for each case.

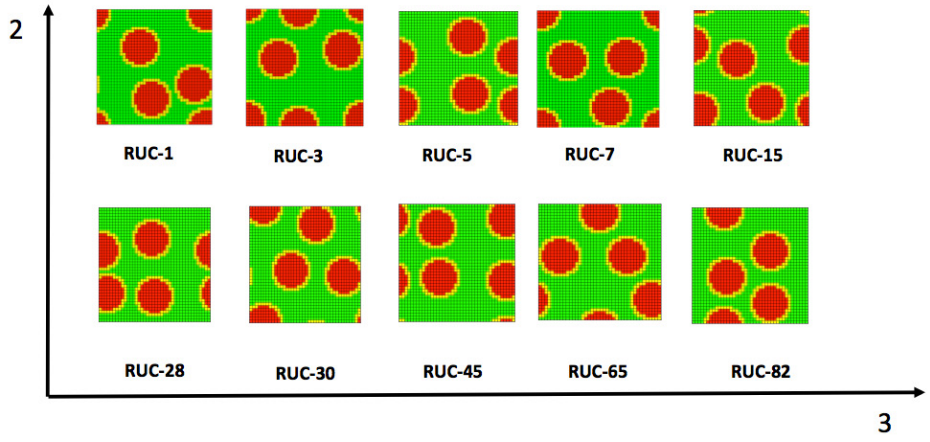

Figure 13.—A sampling of the 100 randomly generated disordered RUC microstructure with four circular fibers within.

TABLE III.—[90] SIC/SIC LAMINATE; 100 SIMULATIONS; 4 CIRCULAR FIBERS

	In-Plane Modulus, Ex (GPa)		In-plane Shear Modulus, Gxy (GPa)		Prop. Limit Stress, PLS* (MPa)		Fatigue Life (60 MPa; R= -1)	
	GMC	HFGMC	GMC	HFGMC	GMC	HFGMC	GMC	HFGMC
Mean Value	101.2	152.4	39.2	69.5	59.3	95.5	4,752	6,673
St. Dev.	13.3	6.3	5.5	1.2	21.8	13.9	10,915	7,024
Range	82.5 – 136	139.7-164.1	31.6 – 53.4	66.3-72.2	38.1 – 105	73.3-124.8	0 - 73,328	23 - 37,983
C.O.V.	13.20%	4.10%	14%	1.70%	36.80%	14.60%	229.68%	105.26%
Sq. Pack	143.4	165	56.2	70.3	110	186.8	111,501	63,771
Hex Pack	126.1	152.7	49.5	71.4	52.7	133	32,466	4,666

TABLE IV.—$[0/90]_s$ SIC/SIC LAMINATE; 100 SIMULATIONS; 4 CIRCULAR FIBERS

	In-Plane Modulus, Ex (GPa)		In-plane Shear Modulus, Gxy (GPa)		Prop. Limit Stress, PLS* (MPa)		Fatigue Life (150 MPa; R= -1)	
	GMC	HFGMC	GMC	HFGMC	GMC	HFGMC	GMC	HFGMC
Mean Value	202.4	227.8	39.2	69.5	149	176.7	1,986,456	2,063,349
St. Dev.	6.7	3.1	5.5	1.2	46.2	20.7	10,384	18,417
Range	193 – 219.7	221.5 – 233.6	31.6 – 53.4	66.3 – 72.2	94.3 – 239	145.2 – 233.4	2,034,392 - 1,9781,110	2,093,137 - 2,032,599
C.O.V.	3.30%	1.40%	14%	1.70%	31%	11.70%	0.52%	0.89%
Sq. Pack	223.4	234	56.2	70.3	182.6	211.2	1,983,623	2,000,196
Hex Pack	215.5	228.7	49.5	71.4	227.9	224.2	2,453,355	2,461,295

Two types of laminates will be examined, unidirectional [90] and cross-ply $[0/90]_s$. Although unidirectional laminates loaded transverse to the fiber direction, i.e., [90], are not employed in practice, this type of laminate will exhibit the greatest sensitivity to microstructural influences and is often the most examined in the literature. Cross-ply laminates are more relevant for practical usage. It should be noted that in a longitudinal [0] composite (i.e., loaded along the fiber direction) the microstructure has minimal to no influence on the response/properties of such a composite. The properties and response in that situation generally depends only upon the volume fractions of each constituent as well as the properties of the constituents themselves. Effective moduli, PLS and fatigue life results, in terms of mean, standard deviation (St. Dev.), range and coefficient of variation (C.O.V.), for all 100 instances simulated by GMC and HFGMC for [90] and $[0/90]_s$ laminates are tabulated in Table III and Table IV, respectively. Also results for square and hexagonally packed, ordered, microstructures are given for each laminate as well.

In general, there is a significant difference between the GMC and HFGMC simulated properties (effective moduli and PLS) as well as fatigue life when dealing with disordered microstructures. This is mainly due to the lack of normal and shear stress coupling within GMC, which is exacerbated by the presence of the weak interface coating around each fiber. Comparing Table III and Table IV results, it is apparent that the C.O.V. is significantly reduced for the cross-ply laminate (with generalization to any fiber dominate laminates, i.e., with [0] plies present) as compared to the [90] laminate for the in-plane transverse modulus and fatigue life, whereas in the case of the in-plane shear modulus and PLS the C.O.V. are very similar. This is reasonable since the in-plane shear modulus is controlled by the fiber properties and fiber volume fraction and the PLS is controlled by the “first ply failure” which in these two

laminates corresponds to the [90] ply as [90] ply fails first in a cross-ply laminate. It is interesting to note that the C.O.V. in fatigue life for the $[0/90]_s$ laminate is less than 1 percent since it is dominated by the cyclic dependent fiber strength which provides significantly longer cyclic life (at least two orders of magnitude) than the cyclic life of the matrix at the given fully-reversed applied load level of 150 MPa (see Figure 4 and Figure 5). Finally, assuming that HFGMC predictions are accurate, it also appears, as expected, that results predicted using an ordered hexagonal packed microstructure agree reasonably well with the HFGMC mean value predictions coming from 100 instances of disordered microstructures for both [90] and $[0/90]_s$ laminates. The only exception appears to be in the case of in-plane shear modulus, PLS and fatigue life for the [90] and $[0/90]_s$ laminates where square packing agrees better.

Figure 14 and Figure 15 show the monotonic stress-strain response for the upper and lower bound disordered instances as well as the square (square symbol) and hexagonal (triangular symbol) ordered microstructure RUCs for the [90] and $[0/90]_s$ laminates, respectively. In both figures, GMC and HFGMC predictions are made using the upper and lower bound RUC instances computed associated with GMC (dashed lines) and HFGMC (solid lines) bounds. Again the variation between the upper and lower bound is significantly greater in the [90] case (Figure 14) as compared with the $[0/90]_s$ laminate case (Figure 15). For both laminates, HFGMC predictions (purple) are the highest when using the upper bound instances obtained from either GMC (RUC-45) or HFGMC (RUC-28). Similarly, GMC predictions (black) are the lowest when using the lower bound instances obtained from either GMC (RUC-15) or HFGMC (RUC-28).

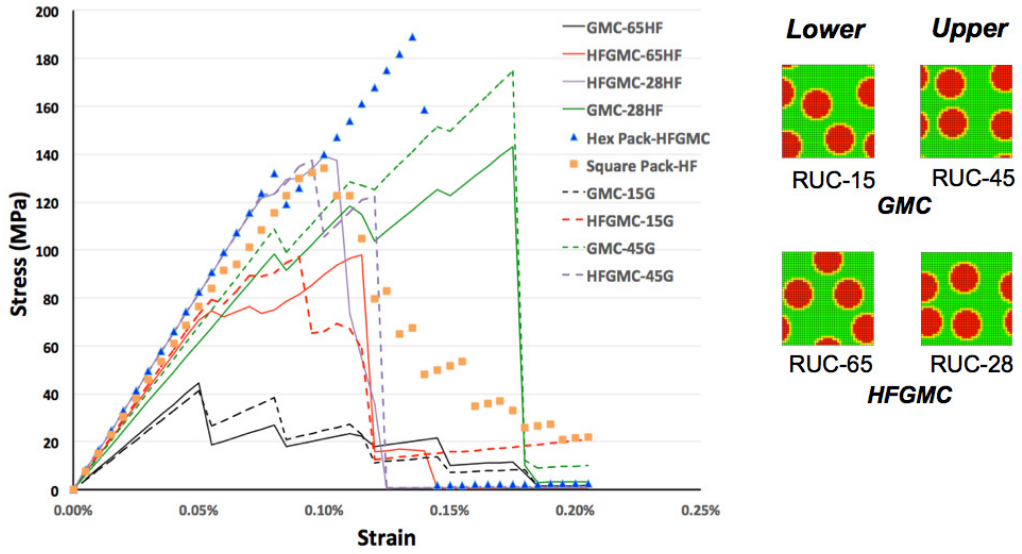

Figure 14.—SiC/SiC [90] laminate stress-strain responses simulated using GMC and HFGMC for the upper and lower bound disordered architectures as well as square and hexagonal ordered architectures.

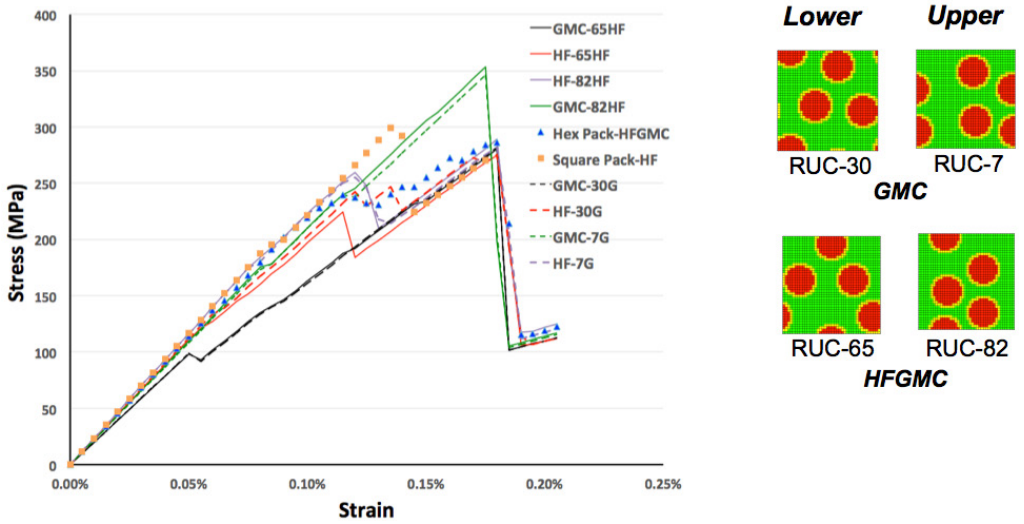

Figure 15.—SiC/SiC [0/90]s laminate stress-strain responses simulated using GMC and HFGMC for the upper and lower bound disordered architectures as well as square and hexagonal ordered architectures.

The influence of microstructure on fatigue life is seen clearly in the fatigue life versus instance scatter plots for [90] and $[0/90]_s$ laminates shown in Figure 16 and Figure 17, respectively. For the [90] layup, see Figure 16, although the predicted fatigue life can vary significantly between GMC and HFGMC for a given instance, the mean values between the two methods only differ by approximately 28.7 percent. Table III indicates that the C.O.V. for fatigue given by GMC is approximately 230 percent while for HFGMC it is 105 percent. In the case of $[0/90]_s$ layups, see Figure 17 - note here the fatigue life is normalized by HFGMC mean value (2,063,349), the difference in predicted fatigue life for any instance between GMC and HFGMC is less than 8 percent while the difference in mean lives is also approximately 3.7 percent. Table IV indicates that the C.O.V. for fatigue given by GMC is approximately 0.5 percent while for HFGMC it is 0.89 percent. Clearly, the [0] ply suppress the microstructure variation observed in a [90] ply (see Figure 16) such that the significantly more computationally efficient GMC method (although not well suited for accurately predicting unidirectional composite disordered microstructures) can be employed efficiently with very good accuracy for $[0/90]_s$ laminates. Note the average computational time for the 100 instances for HFGMC was 1600 sec while GMC was only 6 sec; a 266 times improvement. We believe this conclusion should be extendable to other layups containing [0] plies as well. This will be confirmed in future studies.

Figure 18(a) illustrates multiple S-N curves associated with the minimum (brown line with star), average (red dashed line), and maximum (brown with diamond symbol) lives of 100 random RUCs for a [90] laminate. In addition, a hexagonal packed periodic microstructure RUC (blue line) is also provided in Figure 18. Clearly, this hexagonal RUC matches the mean of 100 runs at higher load levels but as the load decreases the hexagonal RUC provides significantly shorter lives. Consequently, the hexagonal RUC is conservative for all load levels. Also, apparently above 55 MPa the failure mechanism changes from matrix fatigue damage to interface failure. Note this is clear from comparing RUC-69 (minimum response at 60 MPa) and RUC-39 (maximum response at 60 MPa). Yet these responses switch at 55 MPa and below. Figure 18(b) shows the S-N curve for a [0/90] laminate and the scatter in these curves is significantly less than what is observed for a [90] laminate. As mentioned before, the presence of [0] plies in a laminate suppresses the scatter that arises due to microstructure variation.

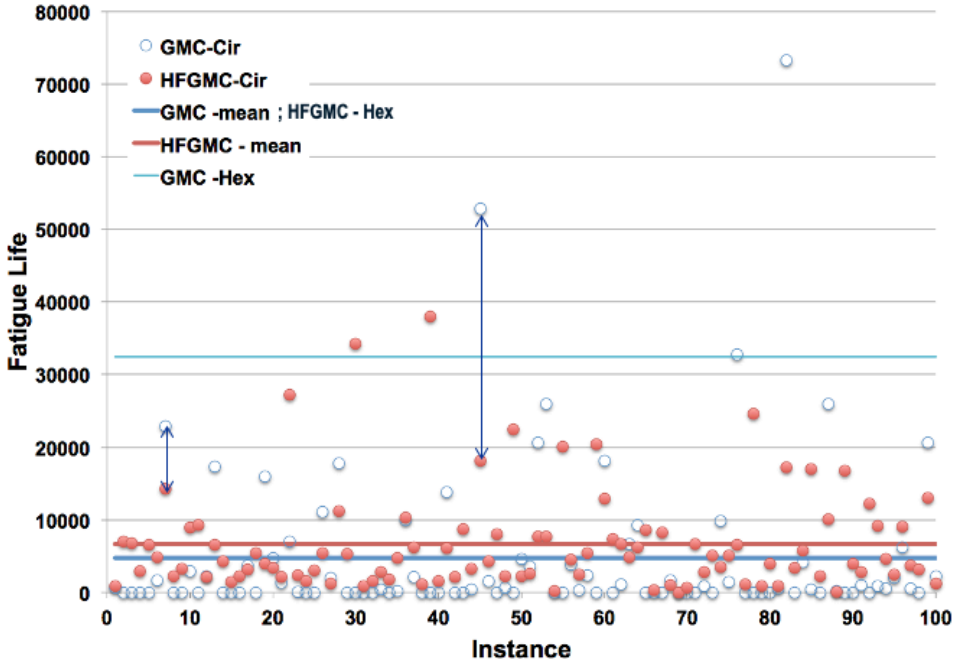

Figure 16.—SiC/SiC [90] laminate, ν_f = 0.28, fatigue life simulated using GMC and HFGMC for 100 random disordered microstructure instances. Loading is uniaxial 60 MPa fully reversed cyclic loading, and applied transverse to the fiber direction. Four fibers are contained within each RUC.

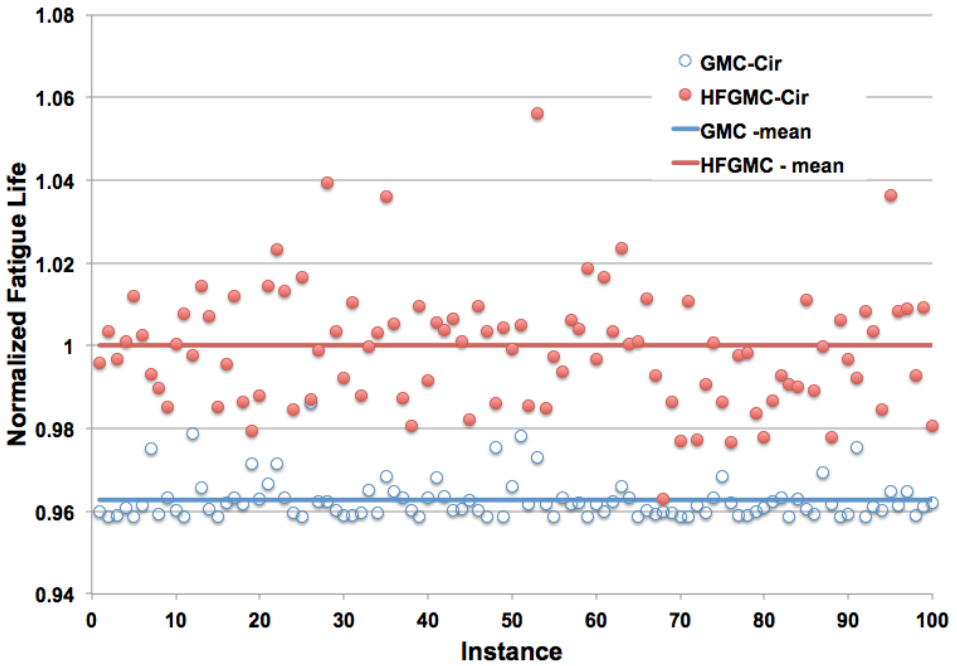

Figure 17.—SiC/SiC [0/90] laminate fatigue life simulated using GMC and HFGMC for 100 random disordered microstructure instances subjected to a uniaxial 150 MPa , fully reversed cyclic applied load. Four fibers are contained within each RUC. Normalization factor is 2,063,349.

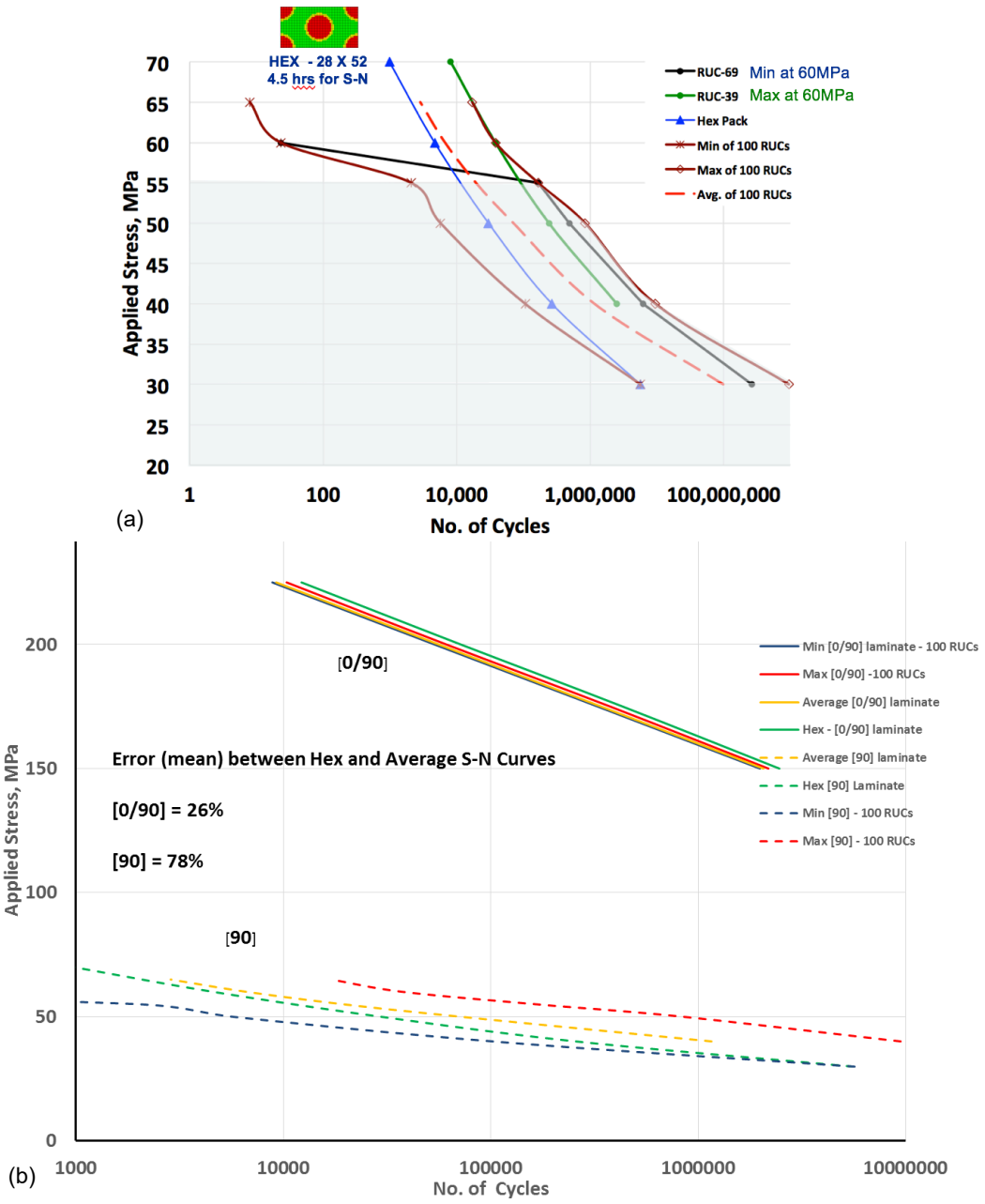

Figure 18.—Fatigue S-N Curve for SiC/SiC (a) [90] laminate and (b) [0/90] laminate, Range of [90] laminate also plotted for comparison; ν_f = 0.28, simulated using HFGMC for 100 random disordered microstructure instances.

Figure 19 illustrates the resulting probability density functions given 4 random fiber (noted as 2x2), 9 random fiber (denoted as 3x3) and 25 random fiber (denoted as 5x5) RUCs loaded uniaxially at 50 MPa. All simulations are conducted using HFGMC micromechanics method and indicate that the three resulting PDF responses are non-normal distributions. Note that as the number of fibers is increased in each RUC the amount of scatter reduces and the mean response approach the mode. The resulting non-normal distribution suggest that when performing design, the mode should be used over that of the mean

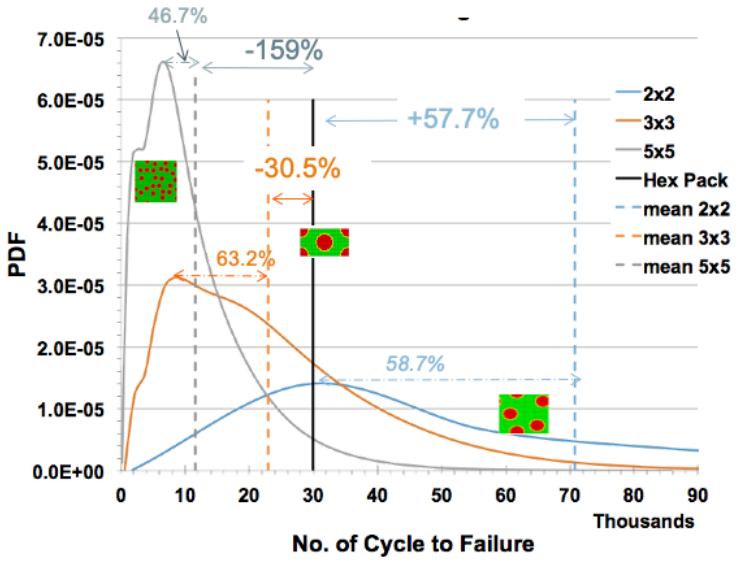

Figure 19.—Simulated fatigue life probability distribution function for a SiC/SiC [90] laminate, v_f = 0.28, using HFGMC for 100 random disordered microstructure instances given 4, 9 and 25 fibers in an RUC subjected to an applied stress of 50 MPa (see Figure 18(a)).

response since it represents the more prevalent life. Also, on average the mode life is approximately 58 percent more conservative than the associated mean life. Lastly, the hexagonal pack RUC (from Figure 8) is shown to match the mode of the 4 fiber RUC and over predict the mode of the 9 fiber RUC distribution by a factor of 3.75. However, a significant speed up 18x and 100x over random RUCs is observed. Note the mean and mode of the fatigue life distribution are even shorter for 25 fiber RUCs, see Figure 19. Additionally, although not shown a coarser hexagonal pack RUC (14x26) was shown to predict a longer life (i.e., 4.6x) than that of the finer (28x52) hex pack RUC yet at a significantly faster (14x) computational speed. Finally, from these results it appears that an ordered HEX RUC provides a good balance between efficiency and fidelity for multiscale modeling. Also, random microstructure variation is significantly reduced when one considers laminated composites where certain percentage of the plies are oriented in the [0] or along the primary loading direction.

Manufacturing Variability: Variable Fiber Diameter/Coating Thickness

The previous section dealt with a single aspect of microstructure variation; fiber center location. Here, in addition to fiber center location variability, variability involving fiber diameter and interface coating thickness will be examined. The primary question to be addressed is whether there is any advantage (relative to moving the mean composite response) in trying to hold the fiber diameter and/or coating thickness constant. This is a practically significant manufacturing question, since it is technologically possible (but requires significant resource investment) to achieve uniform fiber diameter and/or fiber coating thickness. Although, in reality this is a very difficult if not intractable problem to examine experimentally due to the difficulty to control the various sensitive parameters, i.e., fiber volume fraction, fiber diameter, coating thickness, etc., throughout the domain over which the response is being averaged. However, micromechanics enables one to easily control these parameters and assess their sensitivity and influence on the composite response. Therefore, the question is, is it a worthwhile investment of resource?

To answer this, four sets of 100 random disordered microstructures (idealized with four square shape fibers to aid in the automatic generation of the corresponding RUCs) were simulated. Every instance had the same overall fiber volume (28 percent) and interface volume (13 percent) fractions maintained. In this way the effect of volume fraction was eliminated from the study results, which most likely would be extremely difficult to achieve experimentally. Figure 20 illustrates a sampling of twelve RUCs with three RUCs from each set of 100: top row is the baseline (fixed fiber/fixed coating), second (variable fiber/fixed coating thickness), third (fixed fiber/variable coating thickness) and fourth or bottom row (variable fiber and variable coating thickness). Each row provides the microstructure associated with the lowest (LOW), the mean (AVG), and the highest (HIGH) PLS for the given conditions. Note, the range in variations in fiber diameter and coating thickness was taken to be 9.6 to 14.4 μm and 1.28 to 1.9 μm, respectively. This was equivalent to a C.O.V. of 0.2 assuming a uniform distribution from the baseline of 12-μm fiber diameter and 1.26-μm coating thickness. Table V and Table VI show the statistical results (mean, standard deviation, range, and coefficient of variation) for the elastic properties (transverse and shear modulus), PLS and ultimate strength for all four types of simulations given a unidirectional, [90], and cross-ply, $[0/90]_s$ laminate, respectively. Based on the [90] results and due to the additional computational time required to conduct cross-ply laminate cases, only the baseline and fourth-variable fiber/variable coating thickness simulations were done for the $[0/90]_s$ laminate case and shown in Table VI.

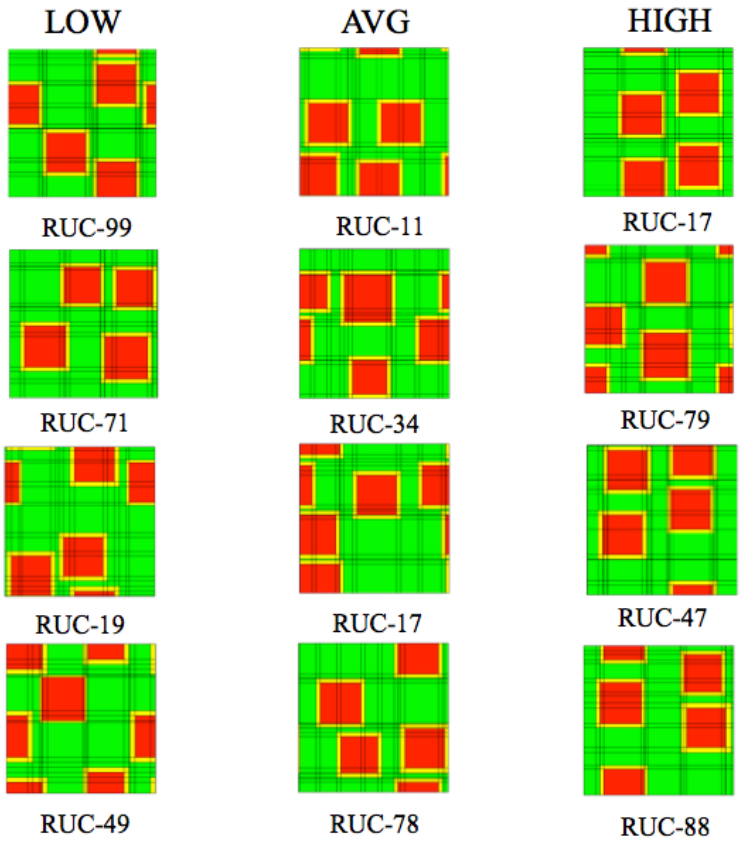

Figure 20.—A sampling of the 100 randomly generated disordered RUC microstructure with four square fibers within; First row - constant fiber diameter and coating thickness, Second row - variable fiber diameter and constant coating thickness, Third row - variable coating thickness and constant fiber diameter, and Fourth row – variable fiber diameter and variable coating thickness. All volume fractions held constant.

TABLE V.—[90] SiC/SiC LAMINATE; 100 SIMULATIONS; 4 SQUARE FIBERS IN THE RUC

	Transverse Modulus, E2 (GPa)				Axial Shear Modulus, G12 (GPa)			
	Baseline	Variable D	Variable Interface t	Variable D & Interface t	Baseline	Variable D	Variable Interface t	Variable D & Interface t
Mean Value	151.7	151.2	152.4	152.6	66.7	66.5	66.9	67.0
St. Dev.	9.6	9.8	9.0	9.9	2.4	2.6	2.2	2.6
Range	133.0 - 168.6	132.0 - 172.0	131.3 - 169.6	131.5 -172.2	59.1 - 72.3	56.7 - 71.2	58.8 - 71.7	59.5 - 73.6
C.O.V.	6.3%	6.5%	5.9%	6.5%	3.5%	3.9%	3.3%	3.9%

	Transverse Prop. Limit Stress, PLS* (MPa)				Transverse Ultimate Stress (MPa)			
	Baseline	Variable D	Variable Interface t	Variable D & Interface t	Baseline	Variable D	Variable Interface t	Variable D & Interface t
Mean Value	91.7	90.1	89.2	90.4	106.9	105.5	106.9	107.5
St. Dev.	31.4	16.2	16.7	18.4	31.4	29.8	30.0	31.2
Range	62.8 - 138.7	64.1 - 131.85	60.6 - 138.0	46.9 - 132.8	64.8 - 184.7	66.6 - 202.8	67.7 - 186.8	57.2 - 183.1
C.O.V.	20.2%	18.0%	18.7%	20.4%	29.3%	28.2%	28.1%	29.0%

TABLE VI.—$[0/90]_s$ SiC/SiC LAMINATE; 100 SIMULATIONS; 4 SQUARE FIBERS IN THE RUC

	In-Plane Modulus, Ex (GPa)		In-Plane Shear Modulus, Gxy (GPa)		In-Plane Prop. Limit Stress, PLS* (MPa)		In-Plane Ultimate Stress (MPa)	
	Baseline	Variable D & Interface t	Baseline	Variable D & Interface t	Baseline	Variable D & Interface t	Baseline	Variable D & Interface t
Mean Value	227.6	228.0	66.8	67.0	287.3	155.3	287.3	289.5
St. Dev.	4.7	4.9	2.3	2.6	15.6	25.2	15.6	18.7
Range	218.7 - 235.9	218.0 - 237.6	59.4 - 72.3	59.4 - 73.7	113.6 - 230.0	110.5 - 222.2	269.4 - 340.2	270.5 - 341.8
C.O.V.	2.1%	2.1%	3.5%	3.9%	17.1%	16.2%	5.4%	6.5%

Clearly in the case of transverse loading of unidirectional composite or a [90] ply, little change is observable (see Table V) in the normal and shear modulus values while strength values show significant variation. As expected, any observed variation is reduced when laminates containing zero plies are considered, see Table VI. Consequently, it appears that devoting any resources to reduce the variability in fiber diameter and/or coating thickness would be unprofitable since it would have minimal impact on shifting the mean of a given static property. Rather, resources should be expended to ensure the desired volume fraction of a given constituent is obtained, since this will shift the mean significantly.

It should be noted that in all microstructural aspects examined the influence of residual stresses due to processing have been ignored. Consequently, the above conclusion may not persist with the inclusion of residual stresses, since microstructural features should strongly influence these local residual stresses, which in turn will impact local failure and thus the PLS and UTS predictions.

Multiscale Modeling of Test Coupons

Multiscale analyses described here were performed using NASA's FEAMAC computer code (Ref. 10). FEAMAC software couples ABAQUS/Standard commercial finite element software package with MAC/GMC micromechanics software for performing multiscale analyses all the way from the constituent to structural scale. In the FEAMAC computer code, ABAQUS calls MAC/GMC to determine

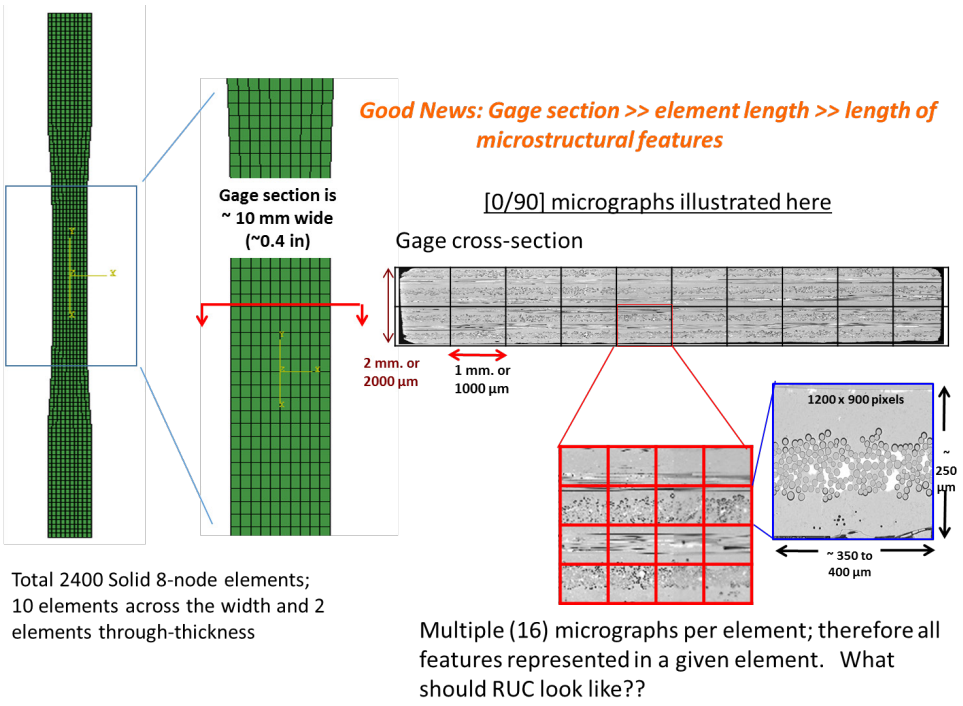

Figure 21.—Test specimen (smooth test coupon) showing a comparison of length scales.

the material response at the integration points within each element(s) or groups of elements identified within the structural FEA model. Any damage or failure is checked at the local level and material stiffnesses are adjusted accordingly. Updated homogenized material constituent properties are then passed on to the structural analyses during the next increment of global loading. MAC/GMC operates as an evolving non-linear anisotropic constitutive model within ABAQUS, representing the composite as a homogenized heterogeneous material. In performing FEAMAC analyses, the user is always confronted with the question of what size RUC or microstructural architecture should be used when performing these analyses? One would like to include or represent the salient microstructural features described above (to represent the multiphased material) yet still have a practical tool for multiscale analyses. Clearly, since these analyses are quite resource intense, one wants to use as simple an RUC as possible (i.e., one with very few subcells and efficient micromechanics, e.g., GMC, analyses) to maintain a proper balance between efficiency and fidelity. It was reasoned in prior sections that to properly account for realistic disordered microstructures, a HEX RUC with HFGMC analyses would provide us with a statistical median of the response and yet keep the analyses computationally manageable. However, when performing multiscale analyses even an ordered HEX RUC would require significant resources of computing power and CPU time. Additionally, one has to keep the length scale of the structural model to length scale of material microstructure in mind when deciding on an appropriate RUC for conducting single or multiscale analyses. Figure 21 shows a finite element mesh of a typical CMC test coupon as well as micrographs of the associated microstructure.

As shown in the figure, a typical gage section is 0.4 in. wide (~ 10 mm) and there are 10 elements across the width of the specimen. Given the size of a typical micrograph and the length of each element as shown, approximately 4 micrographs per ply would fit within each element. It means then, in general, each element's response represents a combination or an average of all the micrographs and their associated features. Thus, one can represent the microstructural features using a simple RUC to represent these features in an average sense. Note the specific RUC representation, be it unidirectional (doubly

periodic) or cross-ply (triply periodic), will be intimately linked with the number elements used to describe the through thickness direction of the structure (or in this case specimen). Usually, the test specimens are 8 ply laminates but just to speed up our computations, the model has two elements through-the-thickness for unidirectional [0] laminates using solid 3-D elements and four elements through-the thickness for [0/90/90/0] laminates when using 3-D solid elements. If using continuum shell elements in the model for a cross-ply laminate, there are two elements through-the-thickness, but each element has a 0 and 90 layer when simulating a cross-ply [0/90/90/0] laminate. As mentioned before, even using an ordered HEX RUC with HFGMC analyses may not be computationally feasible even for this sized structure. This unidirectional specimen, shown in Figure 22, was analyzed using a very simple 5x5 doubly periodic RUC (25 subcells) with square fiber packing shown as an insert in Figure 22 and using the GMC method. The results for the stress-strain curve for a [0] composite are shown in Figure 22. The matrix strength is assumed to *vary spatially*, throughout the gage section, to represent the random occurrence of flaws, cracks, voids and any other irregularity as well as material inhomogeneity. Blue curves represent two simulations of spatially varying matrix strength. These results are compared with a case in which the matrix strength is assumed *spatially constant* so that failure would initiate just outside the gage section where a global stress riser is present. When the matrix strength is assumed to be constant, a sharp drop in the stress strain curve is observed in the simulation, see the green curve in Figure 22. However, the measured data, shown as red curves, does not show such behavior, i.e., the stress-strain curves show a smooth transition. When matrix strength is assumed to be spatially variable, the stress-strain curve shows a similar trend to that observed in the measured data. Obviously, one can calibrate the parameters so as to better match the simulation results with the measured data, but that was not the intent of these analyses. To speed up the analyses, the multiscale computations were performed only in the gage sections (grip areas were excluded from multiscale analyses and an equivalent (effective) anisotropic material property were provided for these elements). Residual stresses due to processing were simulated in these analyses. Run times were approximately 40 min per run on a typical Windows desktop computer using a single CPU[1].

For purely illustrative purposes, straight sided coupons with features were also analyzed using FEAMAC. For example, a unidirectional [0] CMC composite open hole coupon, a cross-ply $[0/90]_s$ CMC open hole coupon and a unidirectional [0] double-notched coupon were analyzed. The purpose of these analyses is to demonstrate the general capabilities of the FEAMAC computer code in solving multiscale problems. In all these analyses, a multiscale GMC analysis employing a 6x8 RUC using two fibers hexagonally packed, with spatially constant strength were employed in all elements. Also, in all these analyses, residual stresses due to processing were simulated prior to the application of mechanical loading. A process or time-temperature profile as shown in Figure 6 was utilized without any heat treatment.

Figure 23 shows the stress-strain curve and damage initiation/progression for a [0] open hole specimen. The model has 1540 solid 3-D elements with two elements through the thickness. The CPU time for the analysis was approximately 2.7 hr. As shown in the figure and expected, damage initiation is localized near the hole and it progresses outward as one would expect. Here matrix strength was assumed to be constant spatially. The damage state marked at three stress magnitudes is also shown in Figure 23. It should be noted that the damage initiates at the load levels marked 1 and 2 but globally no significant deviation from linearity in the global stress-strain curve is observed.

[1] A new thread safe multiscale analysis code, known as NASMAT, capable of being used on a High-Performance Computing (HPC) system, is currently under development at NASA GRC. Version 1.0 was released in Nov 2019.

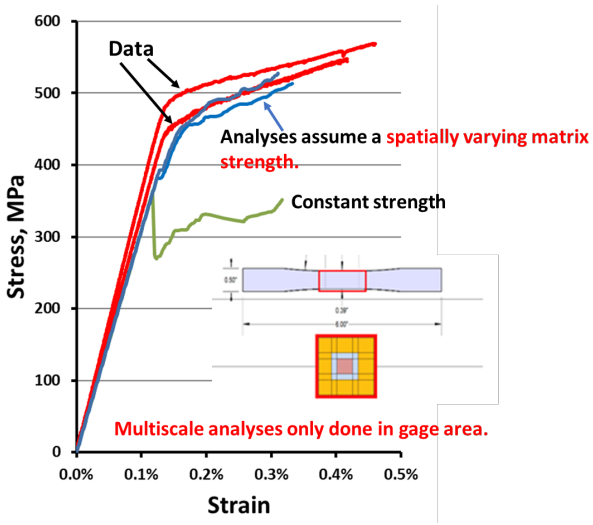

Figure 22.—Response of a unidirectional [0] CMC composite coupon, see (Ref. 1) for data.

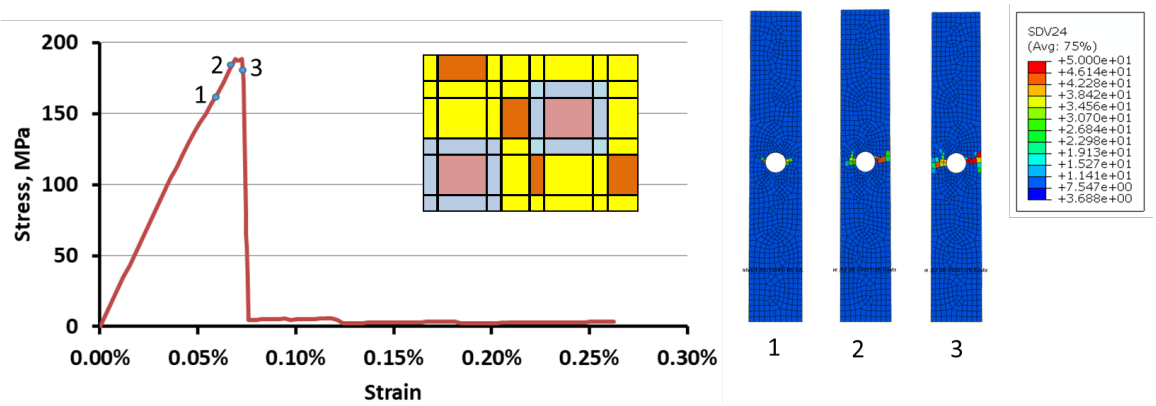

Figure 23.—Response of a unidirectional [0] CMC open-hole coupon (hole diameter/specimen width = 0.4); A four-phase 6x8 RUC used in the analysis is shown in the inset. SDV24 is a measure of damage in the specimen.

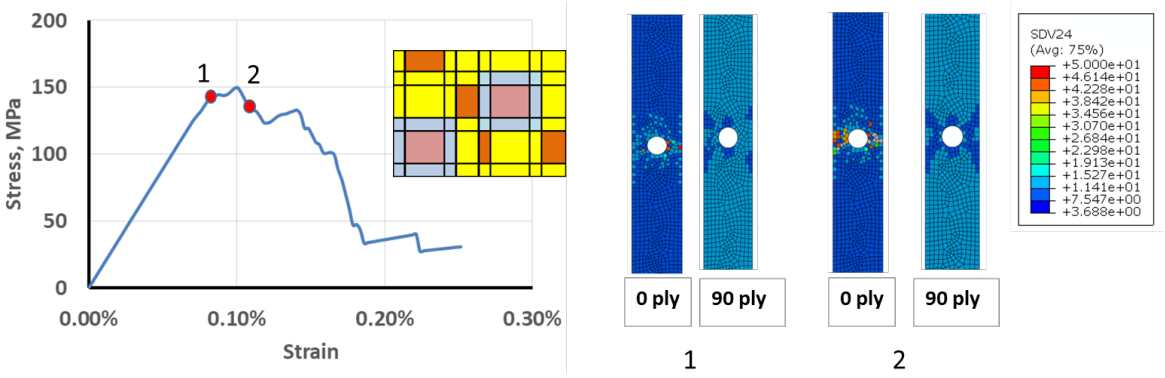

Figure 24.—Response of a cross-ply $[0/90]_s$ laminate open-hole test coupon (hole diameter/specimen width = 0.4); A four-phase 6x8 RUC used in the analysis is shown in the inset. SDV is a measure of damage.

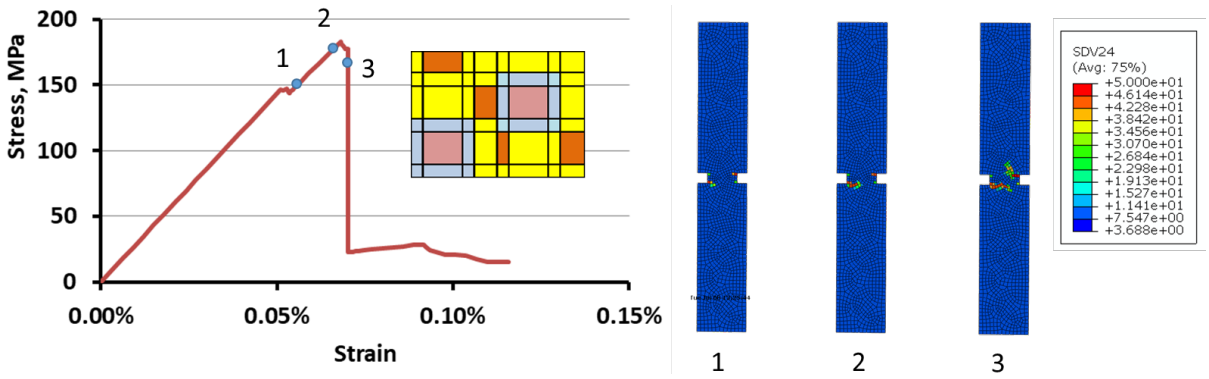

Figure 25.—Response of a unidirectional [0] CMC composite double edge-notched coupon (notch width/specimen width=0.2); A four-phase 6x8 RUC used in the analysis is shown in the inset. SDV is a measure of damage.

In Figure 24, results associated with an open-hole specimen with a $[0/90]_s$ laminate are shown. This model has 2000 continuum shell elements, wherein 2 elements through the thickness are assumed. Each element has two layers, one representing [0/90] plies and other element representing [90/0] plies. Damage initiation and progression is localized near the hole as expected and shown at the right in Figure 24 at the stress levels marked 1 and 2. The CPU time for this analysis was approximately 4.5 hr and a multiscale analysis (using the RUC shown in the insert with spatially constant matrix strength) was performed for all elements.

Figure 25 shows the response of a unidirectional [0] CMC composite double edge notched coupon. This model has 2900 solid 3-D elements with 2 elements through-the-thickness. Analysis took about 5.5 hr of CPU time and multiscale analysis (using the RUC shown in the insert with spatially constant matrix strength) was performed for all elements. As shown in the figure, damage initiation is localized near the notch and the damage progresses towards the center of the coupon as expected. In Figure 25, the damage state is shown on the right side at three stress levels marked 1, 2 and 3.

Macro stress-strain response of both smooth bar (unidirectional and cross-ply) as well as notched specimens were predicted with reasonable efficiency considering that only a single CPU was used to solve the problems. Analyses accounted for residual stresses due to an assumed processing profile and subsequent mechanical analysis. Modeling of notched coupons (open-hole, double-notched) did not involve any additional labor beyond creating the FEM model. Microstructural features (volume fraction, fiber packing, and constituent behavior (both deformation and continuum damage) were included in the FEA constitutive response at each integration point. Results show that damage initiated in the matrix constituent and localized near the notch region as one would expect. These analyses were performed purely to demonstrate the features and capabilities of the FEAMAC computer code to perform multiscale analyses. Obviously, the density of the FEA mesh affects the results. One would also generate denser meshes near the features of interest such as open holes, notches, etc. to better capture stress gradients in those locations. There is always this balance between the fidelity and efficiency of any given analyses. It was also demonstrated, but not shown herein, that multiscale analyses need not be performed over the entire domain of the structure but should be conduct around high stress gradient regions (e.g., within a 2x diameter region of the hole). In this way, the analyses can be conducted even more efficiently without sacrificing the accuracy of the results.

Discussion

CMC response is affected by residual stresses that arise during the processing of composites and manufacturing processes which produce internal material microstructures. The use of micromechanics is important to properly account for any constituent creep/relaxation behavior that takes place during the processing of composites. One can account for residual stresses in an approximate manner (via artificial CTE parameterization) for faster analyses; however, such an approach inhibits accounting for redistribution of residual stresses due to time-dependent effects such as post processing heat treatment performed subsequently or merely time at temperature during creep and relaxation loading. It was also shown that in general, inclusion of residual stresses increases the PLS and thus increases the stress allowable for the composite. However, with this increase in PLS a commensurate decrease in composite ultimate tensile strength is observed due to increases in fiber pre-straining.

Integrated computational materials engineering (ICME) is an integrated approach to the design of products and the materials that comprise them by linking material models at multiple time and length scales. In this paper the statistical influence of microstructure (both ordered and disordered) on the unidirectional and laminated composite effective properties, PLS and fatigue life was investigated for the case of ceramic matrix composites with compliant interfaces. In addition, the advantages/limitations of the micromechanics idealization (GMC or HFGMC) available within the general, synergistic, multiscale-modeling framework for composites (developed by the NASA Glenn Research Center (GRC) and known as MAC/GMC and FEAMAC) when considering microstructural arrangement was discussed. The important findings are summarized:

a) Accounting for spatial variations in composite microstructure within the RUC analyzed is important, as these variations can account for observed statistical variations in both effective properties, PLS and fatigue life.
b) Both micromechanics idealizations can be used to account for this variation; however, the more computationally efficient Generalized Method of Cells (GMC) is significantly more sensitive to microstructure variations, because of the presence of the compliant interface and lack of normal/shear coupling, than is the High Fidelity Generalized Method of Cells (HFGMC).
    i. HFGMC has subcell discretization dependence while GMC does not.
    ii. HFGMC typically predicted higher effective properties, PLS, and lower (higher in the case of disordered) fatigue lives than did GMC for order and disordered microstructures.
    iii. HFGMC ordered - hexagonal fiber packing – provides excellent agreement with the mean values resulting from disordered microstructures for most of the effective properties. However, for failure (PLS and fatigue lives) HFGMC hexagonal fiber packing over estimated mean results of 100 random instances by approximately 30 percent for [90] and 20 percent for $[0/90]_S$ layups. Thus, indicating the need to address disordered microstructures (obtain accurate local fields) when desiring to accurately predict failure of composites.
    iv. Although the fatigue lives predicted by HFGMC and GMC can vary significantly based on individual microstructures, the mean fatigue life value (i.e., averaged over multiple microstructure realizations) for a given RUC discretization (e.g., 4 (20x20) fiber unit cells within the RUC) between HFGMC and GMC is relatively small (< 30 percent). Note, that the actual percentage discrepancy, in the case of disordered microstructures, is highly dependent upon volume fraction and property mismatch between constituents.

c) Transversely loaded unidirectional composites, [90], demonstrated the highest sensitivity to microstructure, whereas for laminates with [0] plies, e.g. $[0/90]_S$, this sensitivity greatly suppressed.
d) Variability in fiber diameter and interface coating had little to no impact on shifting the mean response of an identical composite system with a constant fiber diameter and coating thickness – provided the fiber and interface volume fraction remained fixed.
e) Periodic ordered hexagonal pack RUC approximated the mode of the non-normal distribution resulting from disordered microstructures reasonably well and thus enables a more computationally efficient use of microstructures for design purposes.

A few multiscale analyses were also shown using simple RUCs to demonstrate that micromechanics-based solutions can be performed in reasonable time to provide engineering solutions. Clearly, micromechanics can be effectively utilized to link the material microstructure (e.g., constituent phase properties, volume fraction, fiber packing (ordered or disordered), etc.) to ply/laminate properties (mesoscale) and finally to performance (at the macroscale), in an efficient and accurate manner to enable 'fit-for-purpose' tailoring of the composite material. The ability to localize and homogenize efficiently between scales make MAC/GMC and FEAMAC ideal candidates for ICME simulations in a multiscale environment in which the microstructure can be optimized spatially based on the local loading and environmental history. Finally, extreme caution should be used when adopting/utilizing input constituent (fiber/matrix) properties either from the literature or a given model, as the fidelity of the given model used to obtain those "in-situ material properties" will impact the predictive ability of another model with a different degree of fidelity and assumptions. Currently, work is going on to parallelize the FEAMAC computer code such that while performing multiscale analyses, one will be able to use more complex RUCs and yet perform those analyses efficiently.

References

1. Dunn, D. (2010). The effect of fiber volume fraction in HiPerComp® SiC-SiC Composites. Ph.D. thesis, Alfred University, Alfred, New York.
2. Bednarcyk, B. A., and Arnold, S. M., (2002); "MAC/GMC 4.0 User's Manual, Volume 2: Keywords Manual", TM 2002-212077/Vol 2, 2002.
3. Trias, D., Costa, J., Turon, A., and Hurtado, J. E. (2006). Determination of the Critical Size of a Statistical Representative Volume Element (SRVE) for Carbon Reinforced Polymers. Acta Materialia, 54(13): 3471-3484.
4. Huang, Y., Jin, K. K., and Ha, S. K. (2008). Effects of Fiber Arrangement on Mechanical Behavior of Unidirectional Composites. Journal of composite materials, 42(18): 1851-1871.
5. Maligno, A. R., Warrior, N. A., and Long, A. C. (2009). Effects of Inter-fibre Spacing on Damage Evolution in Unidirectional (UD) Fibre-reinforced Composites. European Journal of Mechanics-A/Solids, 28(4): 768-776.
6. Wang, Z., Wang, X., Zhang, J., Liang, W., and Zhou, L. (2011). Automatic Generation of Random Distribution of Fibers in Long-fiber-reinforced Composites and Mesomechanical Simulation. Materials & Design, 32(2): 885-891.
7. Romanov, V., Lomov, S. V., Swolfs, Y., Orlova, S., Gorbatikh, L., and Verpoest, I. (2013). Statistical Analysis of Real and Simulated Fibre Arrangements in Unidirectional Composites. Composites Science and Technology, 87:126-134.

8. Garnich, M. R., Fertig, R. S., and Anderson, E.M. (2013); "Random Fiber Micromechanics of Fatigue Damage", 54th AIAA/ASME/ASCE/AHS/SC Structures, Structural Dynamics, and Materials Conference, AIAA 2013-1656 , Boston, MA, April 8-11, 2013.
9. Arnold, S.M., Murthy, P., Bednarcyk, B.A., and Pineda, E.J (2015) "Microstructural influence on Deformation and Fatigue Life of Composites Using the Generalized Method of Cells", AIAA SciTech, 2015, 56th AIAA/ASME/ASCE/AHS/SC Structures, Structural Dynamics, and Materials Conference, January 5-9, 2015.
10. Aboudi, J., Arnold, S.M., and Bednarcyk, B.A., (2013); *Micromechanics of Composite Materials: A Generalized Multiscale Analysis Approach*, Elsevier, Inc., 2013.
11. Paley, M. and Aboudi, J., (1992) "Micromechanical Analysis of Composites by the Generalized Cells Model" Mechanics of Materials, 14:127–139.
12. Aboudi, J., Pindera, M.J. and Arnold, S.M. (2002) "Higher-Order Theory for Periodic Multiphase Materials with Inelastic Phases", NASA/TM 2002-211469. Also see IJP, 2003, 19: 805-847.
13. Liu, K. C., and Ghoshal, A. (2014). Inherent Symmetry and Microstructure Ambiguity in Micromechanics. Composite Structures, 108:311-318.
14. Aboudi, J., Arnold, S.M., and Bednarcyk, B.A., (2021); *Practical Micromechanics of Composite Materials*, Elsevier, Inc., 2021.
15. N. E. Dowling, Mechanical Behavior of Materials: Engineering Methods for Deformation, Fracture, and Fatigue, (1999), Prentice Hall, New Jersey
16. J. Lemaitre and Chaboche, J.L., Mechanics of Solid Materials, (1990), Cambridge University Press.
17. Skrzypek, J. and Hetnarski, R. (1993). Plasticity and Creep Theory Examples and Problems. Boca Raton, FL.: CRC Press.
18. Arnold, S.M., and Kruch, S. (1994). Differential Continuum Damage Mechanics Models for Creep and Fatigue of Unidirectional Metal Matrix Composites. International Journal of Damage Mechanics, 3(2): 170-91.
19. Chaboche, J.L. and Lesne, P.M. (1988). A Non-Linear Continuous Fatigue Damage Model, Fatigue Fract. Engng. Mater. Struct., 11(1): 1-7.
20. Wilt, T.E., Arnold, S.M., and Saleeb, A.F. (1997). A Coupled/Uncoupled Computational Scheme for Deformation and Fatigue Damage Analysis of Unidirectional Metal-Matrix Composites. Applications of Continuum Damage Mechanics to Fatigue and Fracture, ASTM STP 1315, D.L. McDowell (Ed.), 65-82.
21. Kruch, S. and Arnold, S. M.., ''Creep Damage and Creep-Fatigue Damage Interaction for Metal Matrix Composites ''Applications of Continuum Damage Mechanics to Fatigue and Fracture, ASTM STP 1351, D.L. McDowell, Ed., American Society for Testing and Materials, pp. 7-28
22. Hansen, L. (2015). Behavior of SiC-SiC Composite Laminates under Multiaxial Load States: Experiments and Simulations. Ph.D. thesis, University of Michigan, Ann Arbor, Michigan.